
EXPERIMENTAL TESTING

8.1 INTRODUCTION

Fieldwork has been carried out to validate theory developed in this thesis. Some of the algorithms described in Chapters 3 and 7 are tested. Four different B-WIM sites have been monitored with the techniques described in Chapter 4:

- The first site, Delgany (Ireland), was used to obtain data to calibrate the Eurocode (EC1.3) for Irish conditions. B-WIM data was recorded for two uninterrupted weeks for this purpose. An experimental procedure to calibrate a B-WIM system in the frequency domain is introduced. The effect of a change of speed on B-WIM accuracy is also discussed.
- The performance of a B-WIM system under harsh climatic conditions was tested in a bridge in Luleå (Northern Sweden). A major trial with a lot of different truck configurations took place as part of the Cold Environment Test (CET) programme coordinated by COST323 (Henau & Jacob 1998). Results obtained from two vehicles used for calibration are presented.
- A B-WIM system was installed in a bridge in Belleville (Eastern France). This is a long span bridge with substantial dynamics and a high traffic density. A fully instrumented truck participated in this experiment as part of the Continental Motorway Test (CMT) programme (Henau & Jacob 1998). The accuracy of a dynamic algorithm is assessed.
- Finally, a bridge in Slovenia was instrumented at different longitudinal and transverse sensor locations. The multiple-sensor B-WIM algorithm is tested with data obtained from this experiment.

The author has taken an active part in the installation of the B-WIM sites in Ireland, Sweden and France while the data from Slovenia was provided by Brady (University College Dublin, Ireland) and ZAG (Slovenian National Building and Civil Engineering

Institute). In Belleville, TUM (Technische Universität München) provided additional data on bridge strains and VTH (Technical Research Centre of Finland) on the wheel forces applied by the instrumented truck. All accuracy tables are based on the accuracy classification system of the COST323 WIM specification (Appendix B).

8.2 DELGANY, SKEWED SHORT SPAN (15 M) SIMPLY SUPPORTED BRIDGE

This bridge is known as the ‘Barry Bridge’ and is located near Delgany, on the N-11, the main Rosslare-Wexford-Dublin route (Southbound carriageway). Data was obtained from May to July 1997 as part of a contract with the Irish National Roads Authority for the calibration of the Eurocode for Irish Conditions. The bridge is a simply supported single span carrying a two lane road in the same direction (There is another two-lane bridge for the Wexford-Dublin direction). The site location is shown in Figure 8.1.

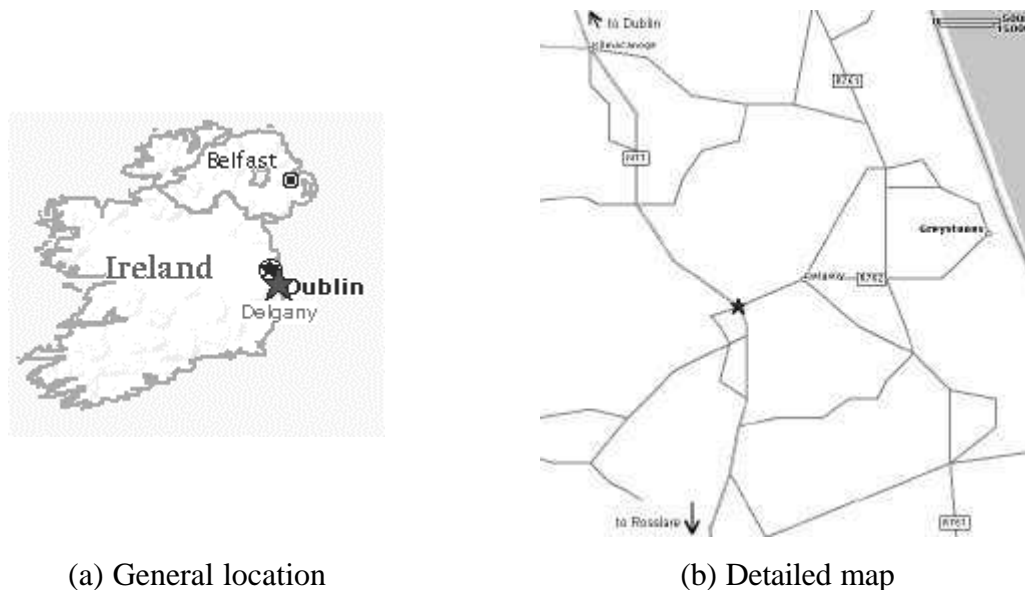


Figure 8.1 – Bridge Location (Delgany)

Reinforced concrete abutments retain embankments at each side. Figure 8.2 gives a general view of the bridge.



Figure 8.2 – Side View of Delgany Bridge

8.2.1 Installation

The bridge is a 16 meter long simply supported ‘beam-and-slab’ structure, composed of 28 precast concrete beams. It has a skew angle of approximately 30 degrees. The dimensions of the bridge are shown in Figure 8.3.

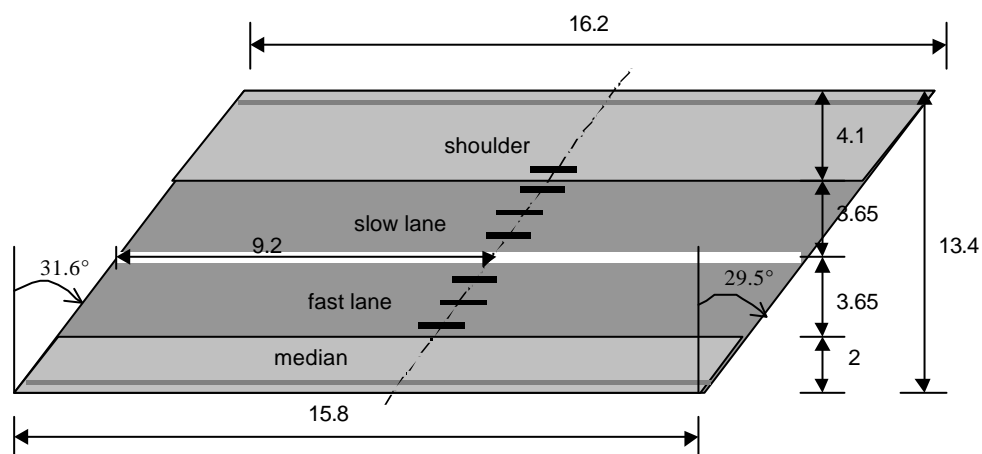


Figure 8.3 - Plan view of Barry Bridge (South-bound carriageway)

Mechanical Strain Amplifiers

The bridge WIM system was installed in one day. It consisted of seven mechanical strain amplifiers (Section 4.2.2) attached to the beams on the soffit and pneumatic axle detectors nailed to the road surface (Section 4.3.1). The amplifiers were used to amplify the strain

induced in the bridge approximately 13 times. This provided a more accurate strain signal by reducing the effects of noise. The amplifiers were placed at approximately mid-span in each beam where the bending moment is relatively large. The exact distance of each amplifier from the abutment is given in Table 8.1. The longitudinal distances were measured from the abutment on the Dublin (North) side of the bridge.

Table 8.1 - Distances of mechanical amplifiers from abutment (Delgany)

Mechanical strain amplifier No.	Beam No.	Longitudinal position (m)	Lane
1	7	9.39	Hard Shoulder
2	10	9.36	Slow
3	13	9.37	Slow
4	16	9.24	Slow
5	19	9.20	Fast
6	22	9.09	Fast
7	25	9.07	Fast

Axle Detectors

Two pneumatic axle detectors (rubber tubes), at a known distance apart, were fixed to each lane (22.827 m in slow lane and 22.657 m in fast lane). The tube before the bridge was placed an average distance of 3.86 m and 1.87 m from the nearest joints in the slow and fast lane respectively. This provided information regarding the speed of the vehicle and the vehicle classification. The axle detectors needed regular maintenance and would not be recommended by the author for long term use.

The rubber tubes were connected to pneumatic convertors which convert the air pulse into electrical analog signals (Figure 8.4(a)). These in turn were connected to the signal conditioning equipment, which conditions the incoming signal. The latter was connected to a portable computer which stored the data (Figure 8.4(b)). The system used to record the strain was developed by National Instruments and is known as the SCXI signal conditioning system which is combined with plug-in boards for data acquisition (Appendix C). The equipment was capable of operating unmanned, though periodic visits were made to the site to back-up data and release memory space from the hard drive as well as to fix the axle detectors, which tended to loosen due to the action of traffic loads. More details of the working of the system can be found in Chapter 4.



(a) Installation of axle detectors



(b) Data Acquisition Equipment

Figure 8.4 – Installation of data collection devices (Delgany)

8.2.2 Testing

The calibration of the system was carried out on the 15th July, 1997 with a 3-axle rigid truck of GVW, 212.3 kN and distances between axles of 4.02 and 1.40 m. The vehicle is shown in Figure 8.5.



Figure 8.5 – Calibration truck used in Delgany

The front axle has a static axle weight of 59.21 kN and the rear tandem 153.09 kN as determined at a certified static scales. Ten significant runs were made at three different speed levels as specified by the European Specification on Weigh-In-Motion of Road Vehicles (2 runs about 55 km/h, 6 runs at 70 km/h and 2 runs at 85 km/h). Both lanes were calibrated although weights were subsequently calculated in only one. Results from a previous calibration of the slow lane on 20th May 1997 are also presented. Accuracy

analysis takes place under extended repeatability conditions (r2) according to the COST323 specification: One vehicle passes several times at different speeds with small variations in lateral position.

Calibration based on a theoretical beam model

The static scale gave only the total weight for the tandem of the calibration truck, so it was assumed that the weight of the individual tandem axles were evenly distributed between the two. Figure 8.6 shows the shape of the theoretical bending moment due to the static loads of the calibration truck according to beam theory. This theoretical response must be scaled down to the corresponding measured record by a calibration factor of 0.683 in order to achieve the correct GVW after applying Equation 3.12. It can be seen the theoretical model does not match well the shape or boundary conditions. The final calibration factor was calculated from all truck crossings.

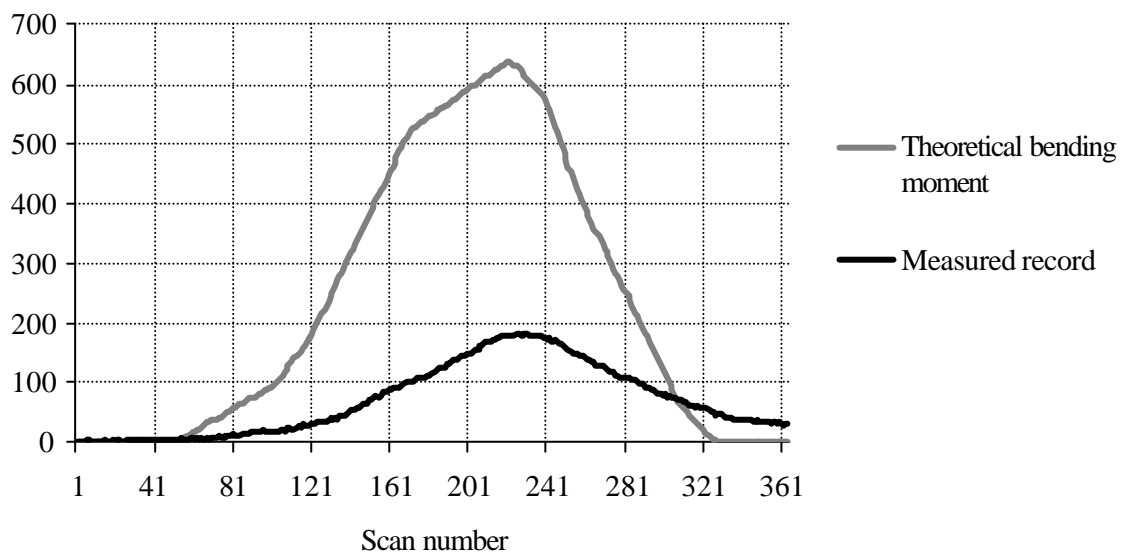


Figure 8.6 – Calibration of theoretical influence line (truck running at 69.48 km/h)
(Delgany)

Tables 8.2, 8.3 and 8.4 give accuracy classes for different identities and three different tests: slow lane in May, and both lanes in July. Accuracy results for the slow lane differ between May and July. The failure of axle detectors and three mechanical strain amplifiers resulted in the installation of new sensors after the calibration in May and the system had to be re-calibrated in July. The most accurate results are obtained in May due to a better adjustment of the amplifiers to the bridge deck. In July, errors were higher in the fast lane

than in the slow lane. The accuracy was poor for axle weights and their values were not used for statistical studies at this site.

Table 8.2 – Accuracy classification by algorithm based on beam model (slow lane - May)

(**n**: Total number of vehicles; **m**: mean; **s**: Standard deviation; **p₀**: level of confidence; **d**: tolerance of the retained accuracy class; **d_{min}**: minimum width of the confidence interval for π_0 ; **p**: Level of confidence of the interval $[-\delta, \delta]$)

Criterion	Relative error statistics				Accuracy calculation				Class Retained
	n	m (%)	s (%)	p ₀ (%)	Class	d (%)	d _{min} (%)	p (%)	
Single axle	10	-42.0	8.35	90.0	E(55)	66	59.6	97.0	E(55)
Group of axles	10	16.22	3.50	90.0	D(25)	28	23.6	98.7	
Gross Weight	10	-0.01	1.95	90.0	A(5)	5	5.0	90.2	

Table 8.3 – Accuracy classification by algorithm based on beam model (slow lane - July)

(**n**: Total number of vehicles; **m**: mean; **s**: Standard deviation; **p₀**: level of confidence; **d**: tolerance of the retained accuracy class; **d_{min}**: minimum width of the confidence interval for π_0 ; **p**: Level of confidence of the interval $[-\delta, \delta]$)

Criterion	Relative error statistics				Accuracy calculation				Class Retained
	n	m (%)	s (%)	p ₀ (%)	Class	d (%)	d _{min} (%)	p (%)	
Single axle	10	-40.2	9.74	90.0	E(60)	72	60.7	98.4	E(60)
Group of axles	10	15.68	2.79	90.0	D+(20)	23	21.5	95.5	
Gross Weight	10	0.09	2.37	90.0	B+(7)	7	6.1	94.8	

Table 8.4 – Accuracy classification by algorithm based on beam model (fast lane - July)

(**n**: Total number of vehicles; **m**: mean; **s**: Standard deviation; **p₀**: level of confidence; **d**: tolerance of the retained accuracy class; **d_{min}**: minimum width of the confidence interval for π_0 ; **p**: Level of confidence of the interval $[-\delta, \delta]$)

Criterion	Relative error statistics				Accuracy calculation				Class Retained
	n	m (%)	s (%)	p ₀ (%)	Class	d (%)	d _{min} (%)	p (%)	
Single axle	10	-62.3	9.75	90.0	E(80)	96	82.8	98.8	E(80)
Group of axles	10	21.50	9.08	90.0	E(40)	44	40.6	94.4	
Gross Weight	10	-1.89	7.62	90.0	D+(20)	20	19.8	90.5	

The errors in the estimation of static weights for all runs are illustrated in Figure 8.7. Front axle and rear tandem are underweighed and overweighed respectively.

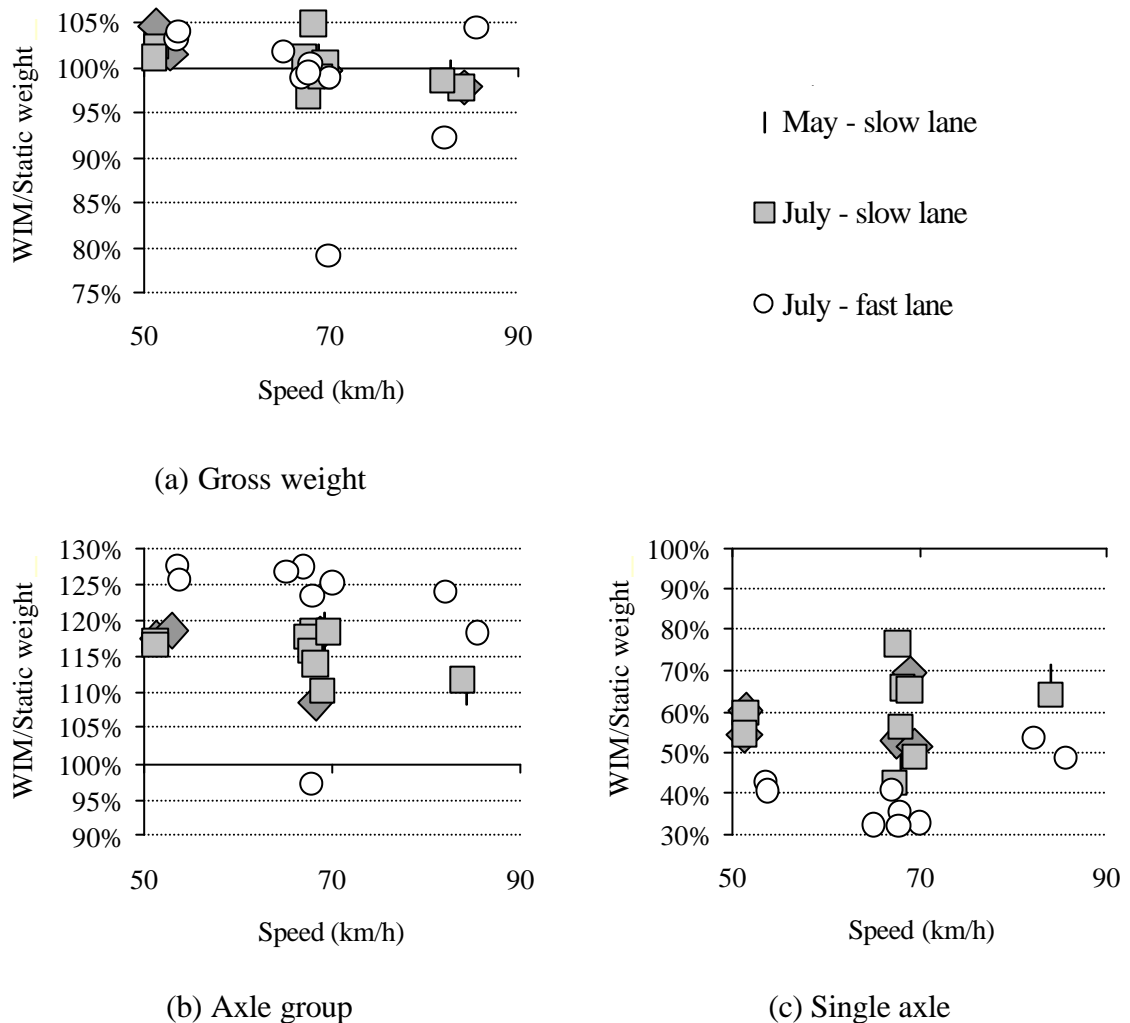


Figure 8.7 – Errors in weights by using a theoretical beam model (Delgany)

Calibration based on an experimental influence line

Accurate influence lines are very important in the overall accuracy of a B-WIM system. Ideally, it should be possible to make a direct calculation of the influence line in stiff bridges (high first natural frequency and low dynamic amplitudes). That is, when there is only one axle on the bridge, if the masses of the calibration truck are known, it is possible to know the value of the influence line from the measured strain record. Then, when a second axle appears on the bridge, the contribution of this second axle to the measured strain can be obtained from the known values of the influence line (already calculated when the first axle passed by that point). As the load effect caused by a second axle on the

bridge is known, the values of the influence line at the new locations of the first axle can be obtained readily by discounting the effect of the second axle. The same procedure could be applied to more axles entering the bridge. In practice, this procedure is very sensitive to the small magnitude of the strains at the start of the bridge and significant errors are introduced in the first steps of the calculation making this approach prone to error.

Hence, the search of the influence line is carried out in such a way that the sum of the effect of all axles matches the measured strains as close as possible. Generally, a theoretical influence line is tested initially and then modifications are done on this curve to improve accuracy (Section 3.5.1). The final adjustment might not be adequate for every single truck as deviations take place due to bridge and truck dynamics.

Alternatively, the author suggests calculating the influence line in the frequency domain as proposed in Section 7.2.2. The spectrum of the influence line is obtained by calculating the unit contribution of all readings to a given frequency. The limitations of a direct calculation in the time domain or the inconvenience of an experimental adjustment, point by point, are overcome. Accordingly, by applying complex arithmetic to Equation 7.5:

$$H_u(f) = \frac{H_m(f)}{\sqrt{(W_1 + W_2 \cos(-fn_1) + \dots + W_r \cos(-fn_{r-1}))^2 + (W_2 \sin(-fn_1) + \dots + W_r \sin(-fn_{r-1}))^2}} \quad (8.1)$$

$$\mathbf{a}_u(f) = \mathbf{a}_m(f) - \tan^{-1} \left(\frac{W_2 \sin(-fn_1) + \dots + W_r \sin(-fn_{r-1})}{W_1 + W_2 \cos(-fn_1) + \dots + W_r \cos(-fn_{r-1})} \right) \quad (8.2)$$

where

- $H_m(f)$: Spectrum magnitude of total measured strain,
- $H_u(f)$: Spectrum magnitude of the strain response due to a moving unit load,
- $\mathbf{a}_m(f)$: Spectrum phase of total measured strain,
- $\mathbf{a}_u(f)$: Spectrum phase of the strain response due to a moving unit load,
- W_i : Weight corresponding to axle i ,

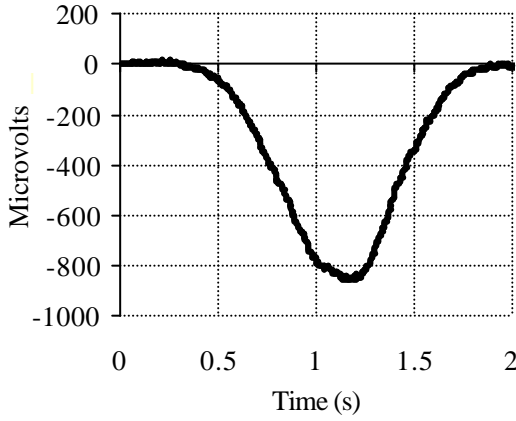
r : Number of axles,

n_i : Number of readings between the first axle and axle $(i+1)$,

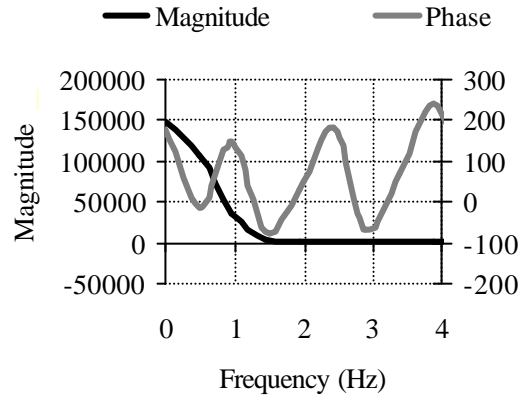
f : Frequency, as $f=2\pi k/N$, where k (0,1,2,...) represents the k^{th} harmonic of the sample.

N = Number of strain readings induced by a vehicle crossing the bridge.

Once the spectrum due to a unit load is obtained, the influence line can be obtained in the time domain through the real part of the inverse transform of $\bar{H}_u(f)$. The process is illustrated in Figures 8.8 and 8.9. Figure 8.8(a) shows the total strain measured for a three-axle truck travelling at 52.85 km/h, and Figure 8.8(b) the corresponding spectrum $\bar{H}_m(f)$.



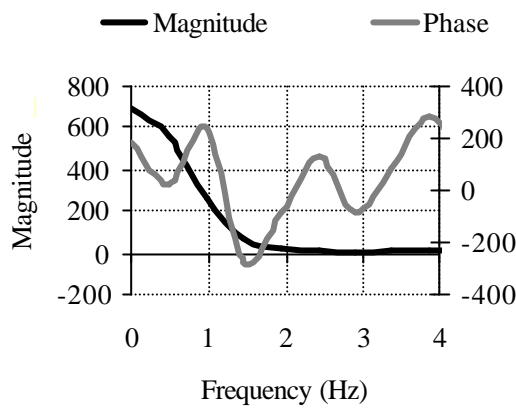
(a) Original record at 52.85 km/h



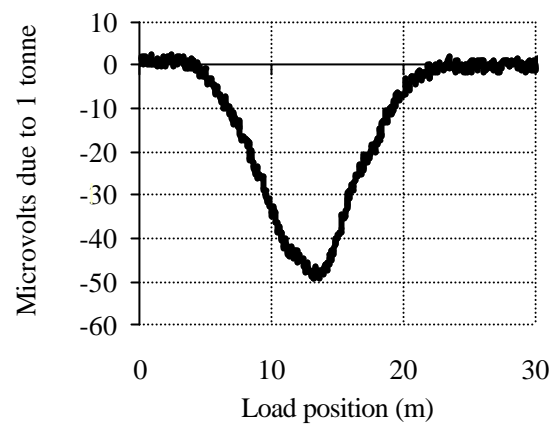
(b) Spectra of record in (a)

Figure 8.8 – Calculation of DFT of the original record (Delgany)

The spectra due to a unit load, $\bar{H}_u(f)$ (Figure 8.9(a)), can be calculated from spectra in Figure 8.8(b) by applying Equations 8.1 and 8.2. The influence line in the time domain is given in Figure 8.9(b) and it is obtained by inverse transform of the spectrum $\bar{H}_u(f)$ in Figure 8.9(a).



(a) Spectra due to a unit load



(b) Experimental influence line

Figure 8.9 – Calculation of spectra due to a unit load and experimental influence line
(Delgany, May 1997)

The levels of accuracy achieved with the influence line in Figure 8.9(b) are given in Table 8.5. Compared to the theoretical beam model, there is an improvement in overall accuracy from E(55) to C(15).

Table 8.5 – Accuracy classification (experimental influence line at 50 km/h) (May) (r2)

(**n**: Total number of vehicles; **m**: mean; **s**: Standard deviation; **p₀**: level of confidence; **d**: tolerance of the retained accuracy class; **d_{min}**: minimum width of the confidence interval for π_0 ; **p**: Level of confidence of the interval $[-\delta, \delta]$)

Criterion	Relative error statistics				Accuracy calculation				Class Retained
	n	m (%)	s (%)	p ₀ (%)	Class	d (%)	d _{min} (%)	p (%)	
Single axle	10	-2.30	6.88	90.0	C(15)	20	18.1	93.6	C(15)
Group of axles	10	0.92	1.51	90.0	A(5)	7.14	4.2	99.6	
Gross Weight	10	0.02	1.50	90.0	A(5)	5	3.8	97.2	

Accuracy can be further improved by obtaining the final influence line through an average of all calibration runs. A low pass filter can also be used to remove noise interference (50 Hz) but an excessive 4 Hz hardware filter was applied while acquiring data in Delgany. This filter does not allow for a recovery of the original signal and undoubtedly it had a negative effect on accuracy by cutting off frequency components of the static response.

Due to the smoothing action of the filter, results are expected to improve if using a separate influence line for each range of speeds. The calibration of a run at 68.94 km/h results in the influence line shown in Figure 8.10.

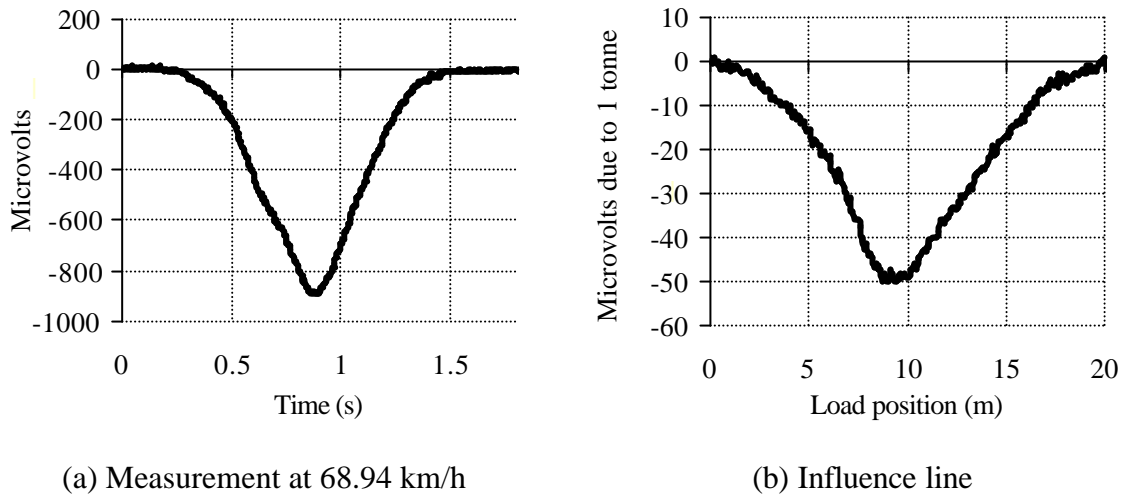


Figure 8.10 - Calibration of slow lane at 68.94 km/h (Delgany, May 1997)

Table 8.6 gives accuracy classes if the 6 runs at about 70 km/h are analysed in full repeatability conditions. The most accurate class, A(5), is obtained for every single criterion.

Table 8.6 – Accuracy classification (experimental influence line at 70 km/h) (May) (r1)

(**n**: Total number of vehicles; **m**: mean; **s**: Standard deviation; **p₀**: level of confidence; **d**: tolerance of the retained accuracy class; **d_{min}**: minimum width of the confidence interval for π_0 ; **p**: Level of confidence of the interval $[-\delta, \delta]$)

Criterion	Relative error statistics				Accuracy calculation				Class Retained
	n	m (%)	s (%)	p ₀ (%)	Class	d (%)	d _{min} (%)	p (%)	
Single axle	6	-2.39	1.53	89.6	A(5)	8	6.2	97.5	A(5)
Group of axles	6	0.78	0.69	89.6	A(5)	7.14	2.5	100.	
Gross Weight	6	-0.10	0.56	89.6	A(5)	5	1.7	99.9	

If all runs are analysed with the influence line derived from calibration at 70 km/h (instead of the 50 km/h run from Figure 8.9(a) - both shapes will be slightly different due to the filter), accuracy classes are as shown in Table 8.7. The results are less accurate than in Table 8.6. The same influence line is used for calculations in Tables 8.6 and 8.7, but the

latter considers all runs, not only those at the speed that influence line has been obtained. Overall accuracy decreases to C(15) due to the poorer estimation of individual axle weights. Hence, it can be seen that results can be improved by using an influence line for each range of speeds when having data filtered at a low frequency.

Table 8.7 – Accuracy classification (experimental influence line at 70 km/h) (May) (r2)

(**n**: Total number of vehicles; **m**: mean; **s**: Standard deviation; **p₀**: level of confidence; **d**: tolerance of the retained accuracy class; **d_{min}**: minimum width of the confidence interval for π_0 ; **p**: Level of confidence of the interval $[-\delta, \delta]$)

Criterion	Relative error statistics				Accuracy calculation				Class Retained
	n	m (%)	s (%)	p ₀ (%)	Class	d (%)	d _{min} (%)	p (%)	
Single axle	10	0.85	7.48	90.0	C(15)	20	19.1	91.7	C(15)
Group of axles	10	-0.30	1.56	90.0	A(5)	7.14	4.0	99.6	
Gross Weight	10	0.02	1.45	90.0	A(5)	5	3.7	97.7	

The calibration of the slow lane in July 1997 is shown in Figure 8.11.

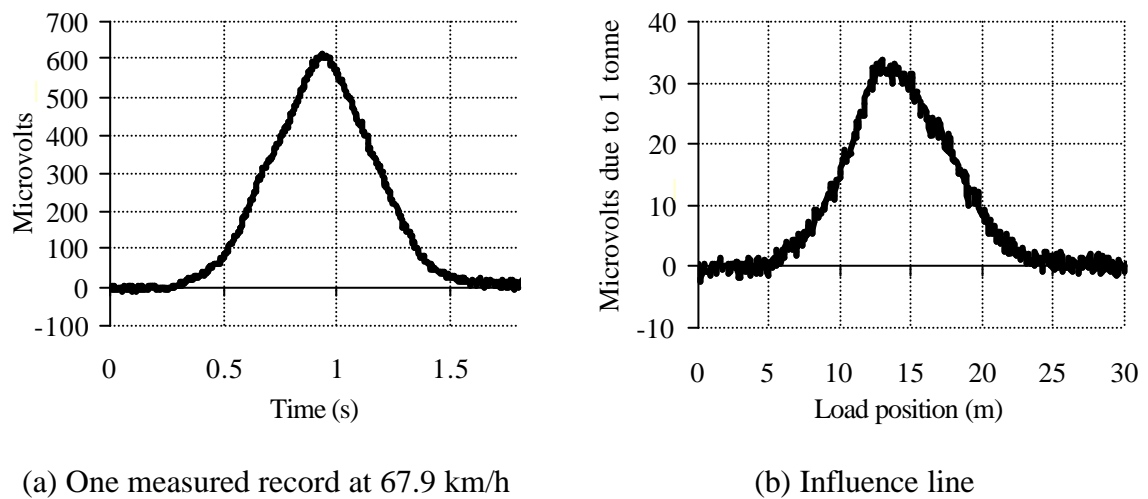


Figure 8.11 – Calibration of slow lane (Delgany, July 1997)

Accuracy classes when using the influence line of Figure 8.11(b) for calibrating the ten July runs are given in Table 8.8. Compared to the theoretical beam model, accuracy in single axles is improved from E(60) to E(40), and accuracy in group of axles from D+(20) to B+(7). Compared to the calibration in May, accuracy in July decreases due to a poorer

resolution for the installation in July. This can be seen in Figures 8.10 and 8.11 (signal to noise ratio lower in July).

Table 8.8 – Accuracy classification (experimental influence line) (slow lane) (July) (r2)

(**n**: Total number of vehicles; **m**: mean; **s**: Standard deviation; **p₀**: level of confidence; **d**: tolerance of the retained accuracy class; **d_{min}**: minimum width of the confidence interval for π_0 ; **p**: Level of confidence of the interval $[-\delta, \delta]$)

Criterion	Relative error statistics				Accuracy calculation				Class Retained
	n	m (%)	s (%)	p ₀ (%)	Class	d (%)	d _{min} (%)	p (%)	
Single axle	10	9.17	14.55	90.0	E(40)	48	40.9	95.3	E(40)
Group of axles	10	-3.46	2.66	90.0	B+(7)	10	9.1	94.2	
Gross Weight	10	0.06	2.65	90.0	B+(7)	7	6.8	91.4	

The calibration of the passing lane in July 1997 is shown in Figure 8.12.

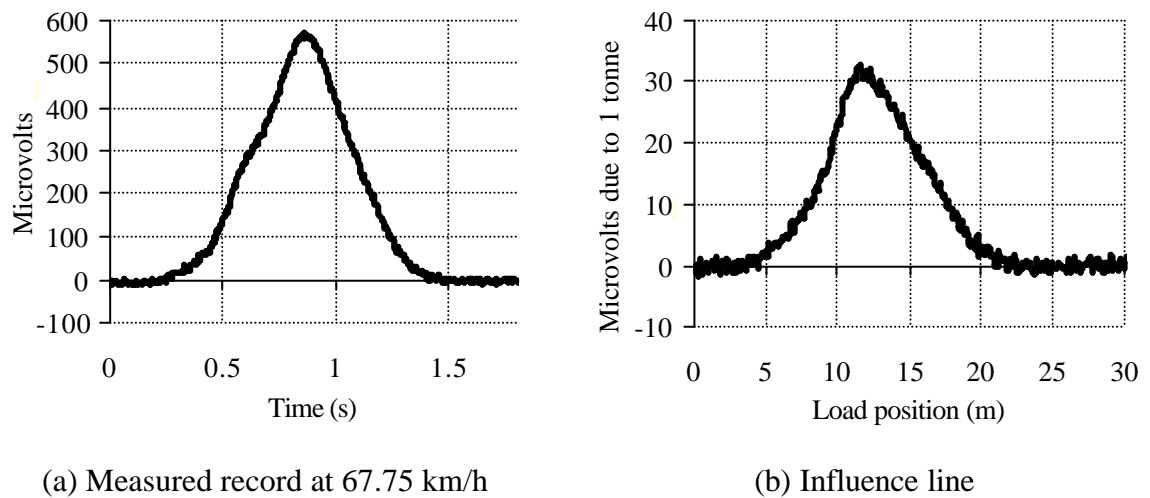


Figure 8.12 – Calibration of fast lane (Delgany, July 1997)

Table 8.9 gives the corresponding accuracy classes obtained for this lane. Accuracy for gross weight is in class B(10) while the calibration using a theoretical beam model only reaches D+(20).

Table 8.9 – Accuracy classification (experimental influence line) (passing lane) (July) (r2)

(**n**: Total number of vehicles; **m**: mean; **s**: Standard deviation; **p₀**: level of confidence; **d**: tolerance of the retained accuracy class; **d_{min}**: minimum width of the confidence interval for π_0 ; **p**: Level of confidence of the interval $[-\delta, \delta]$)

Criterion	Relative error statistics				Accuracy calculation				Class Retained
	n	m (%)	s (%)	p ₀ (%)	Class	d (%)	d _{min} (%)	p (%)	
Single axle	10	0.62	19.75	90.0	E(50)	60	50.4	95.5	E(50)
Group of axles	10	-0.05	5.15	90.0	C(15)	18	13.1	97.9	
Gross Weight	10	0.14	3.78	90.0	B(10)	10	9.6	91.4	

All results are represented in Figure 8.13.

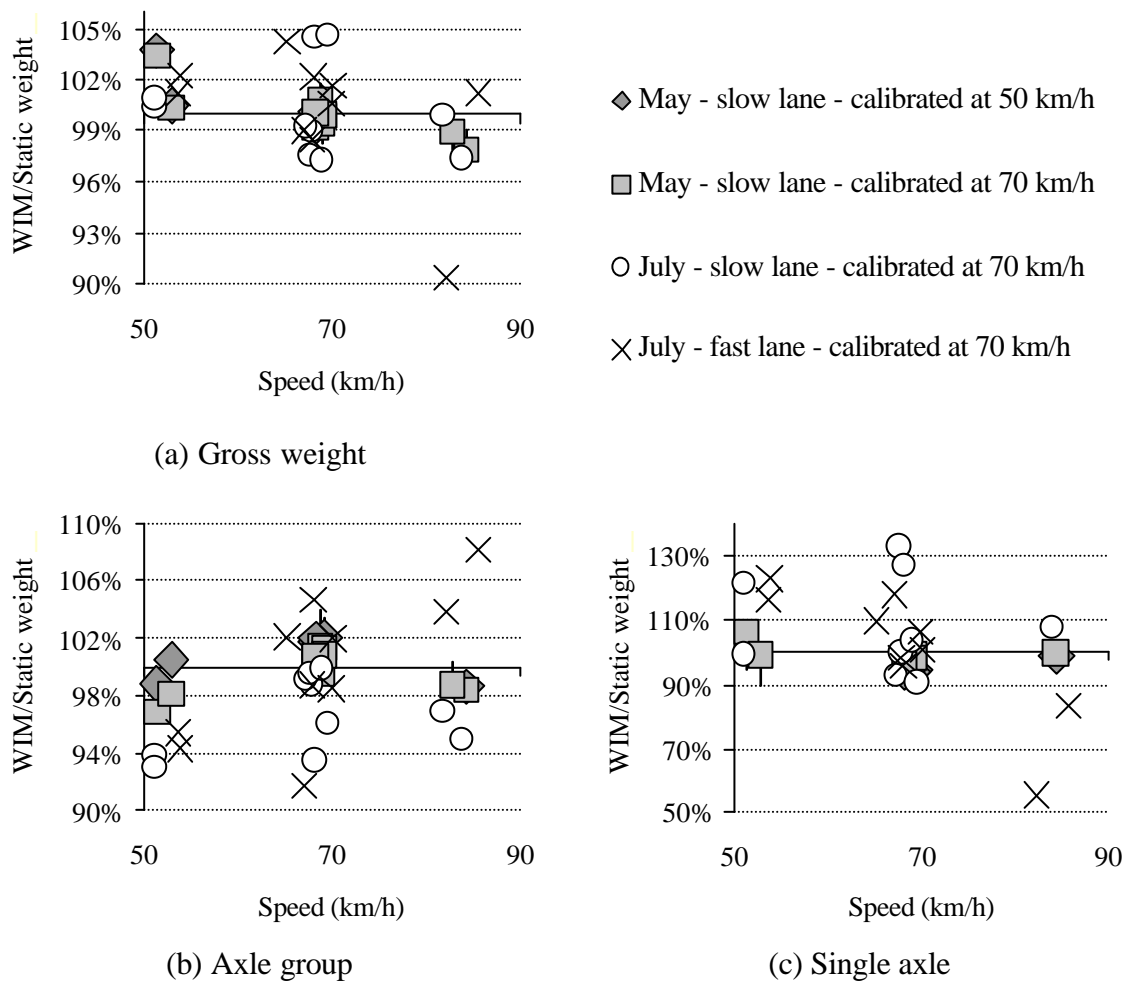


Figure 8.13 – Errors in weights by using calibration in frequency domain (Delgany)

Inaccuracy generally increases when checking results in a speed different from the calibration speed (influenced by inappropriate filtering). The passing lane is the most sensitive to the changes of each run due to the smaller and narrower strain response obtained for this lane.

8.2.3 Traffic Statistics

Fourteen days of South-bound data was collected at the Delgany site between May 20th and July 3rd, 1997 in order to calibrate the Irish bridge load model. Voltage data was recorded continuously on site into 11 channels: 4 from the rubber tubes on the road, and 7 from the strain gauges on the bridge deck. Labview software was used during data acquisition while post-processing was carried out using purpose-written programs in the C language, converting the original voltage information into times and strains for both lanes (Section 4.4.3 and Appendix D). A time was stored for each axle at each tube, and strain was stored for the entire period that a vehicle was on the bridge. Some general statistics on the number of vehicles classified and weighed by the author in twelve days of recording are given in Figure 8.14.

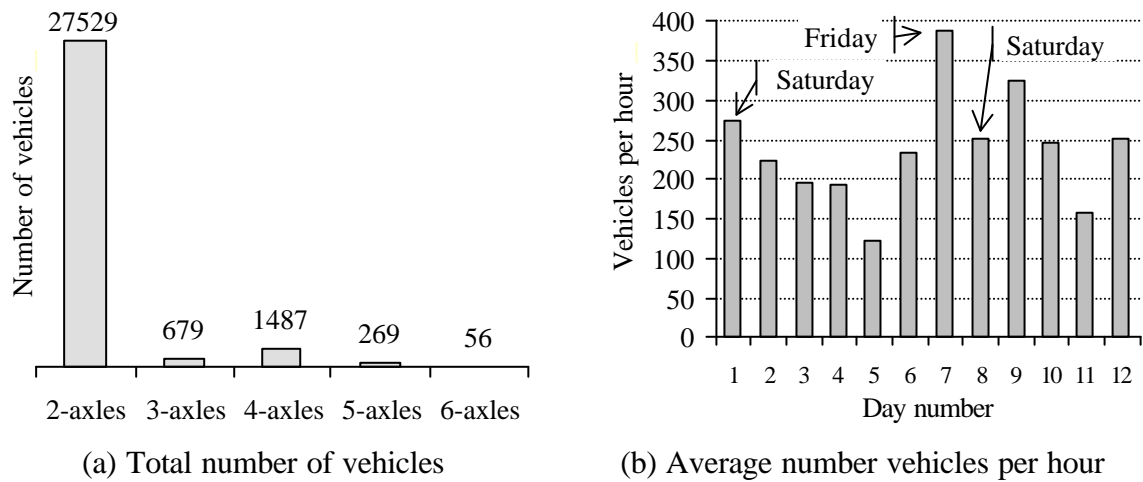
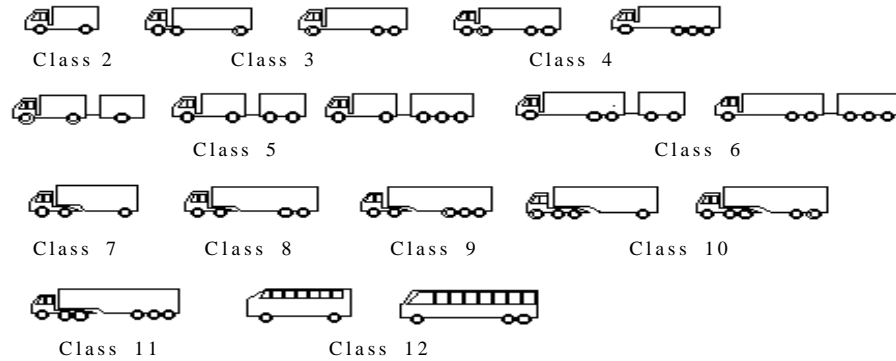


Figure 8.14 – Statistics on the sample in the N11 (Delgany)

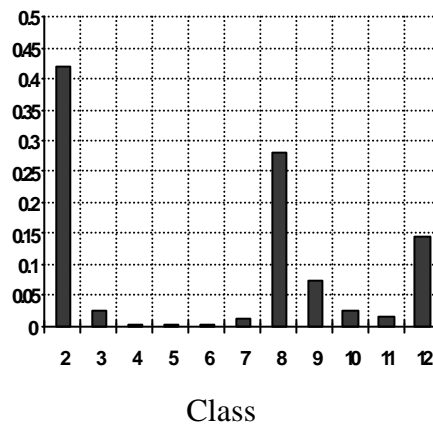
A distribution of the composition by class of Irish truck traffic at the three sites can be seen in Figure 8.15. Vehicles with gross weight less than 3500 kg (i.e., cars and light vans) are grouped in Class 1. In traffic flow modelling for bridges, such vehicles are considered important only for the spacing they represent between larger vehicles in traffic jam

situations (O'Brien et al. 1998b). It is clear that the largest proportion of traffic is made up of the rigid Class 2 vehicles.



(a) Vehicle classification system




Intensity



(b) Histogram for N11

Figure 8.15 - Irish truck traffic composition for sample periods (after O'Brien et al. 1998b)

The 'normal' load model specified in EC1.3 is illustrated in Figure 8.16. It consists of uniformly distributed loading and a bogie of four point loads in each lane. The intensities of load can be adjusted by the relevant national authority through 'alpha-factors' appropriate to local traffic conditions on given road classes. As result of the WIM data collected in Delgany and two other Irish sites, O'Brien et al (1998b) recommends an alpha factor of about 1.3 for all 1-lane bridges. No reduction below unity is recommended in the alpha factors for all 2, 3 and 4-lane bridges.

Lane 1	 <div>Point loads of total intensity $600\alpha_{Q1}$</div>	Uniformly distributed loading of intensity $9a_{q1}$
Lane 2	 <div>Point loads of total intensity $400\alpha_{Q2}$</div>	Uniformly distributed loading of intensity $2.5a_{q2}$
Lane 3	 <div>Point loads of total intensity $200\alpha_{Q3}$</div>	Uniformly distributed loading of intensity $2.5a_{q3}$

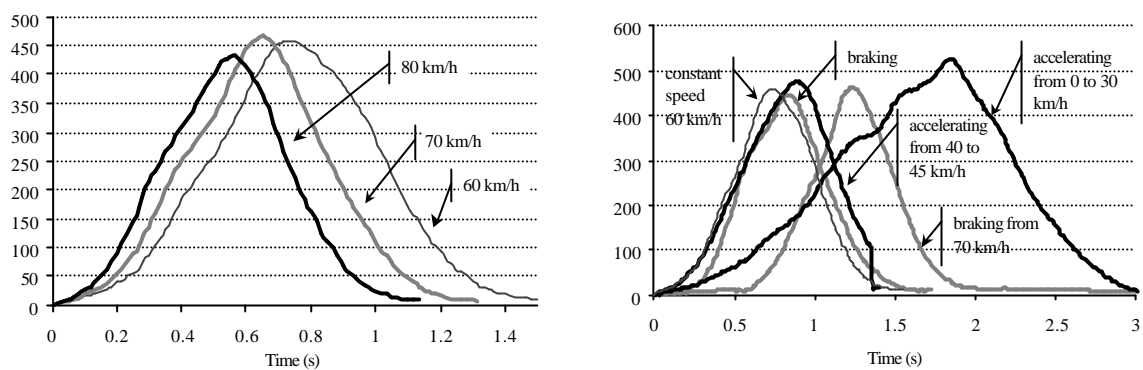
Other Lanes & Remaining Area: Uniformly distributed loading = $2.5a_q$

Figure 8.16 - EC1.3 Normal load model: plan view of loadings in each lane with intensities of loading expressed as a function of the alpha factors (O'Brien et al 1998b)

Individual axle weights by the B-WIM system installed in Delgany are not very accurate. According to O'Brien et al (1998b), while axle spacing can be important, the distribution of weights between axles is not considered to be a significant factor in the calculation of bridge load effects (bending moments and shear forces). At the N11 site, only the gross weights were used. For the purposes of the simulations to calculate 'alpha-factors', typical distributions of the gross weight between the axles were adopted based on those determined at the other Irish WIM sites. This approximation is considered by O'Brien et al (1998b) to not be of such inaccuracy as to invalidating the conclusions.

8.2.4 Influence of Braking Forces on Accuracy

Most B-WIM algorithms are based on an average speed along the bridge that is assumed to be constant. Sudden braking on a bridge can cause a dynamic amplification from 10 to 20% over a road in good condition or from 25 to 30% in poor condition (Major 1980). The Delgany bridge is at a turn on the road and hence the B-WIM site is tested for a strong change in speed along the bridge. Data was collected during September 1996 to analyse the maximum bending in abutments due to horizontal forces (González 1996). Strains were also collected from the bridge deck and the results are shown in Figure 8.17. Five mechanical strain amplifiers were installed about midspan and data was acquired at 60 Hz. A 4 Hz hardware filter was applied.



(a) Bridge response at constant speed

(b) Bridge response at changing speed

Figure 8.17 – Bridge response in the presence of horizontal forces

Bridge response is smaller for higher speeds (80 km/h), while it is closer to the static response for speeds lower than 70 km/h (Section 5.3). Only when the vehicle is imposed a maximum acceleration from nearly null speed at the start of the bridge, a significant deviation from the other runs appears. Hence, the assumption of an average speed is acceptable for most traffic conditions in short span bridges such as Delgany, even in cases of sudden change in speed.

8.3 LULEÅ, TWO SPAN (15 m EACH) INTEGRAL BRIDGE

Tests on the durability of WIM systems in cold climates were organised by the Swedish National Road Administration (SNRA) as part of the CET programme that took place in Northern Sweden, 150 km south of the Arctic Circle (Figure 8.18(a)), from June 1997 to June 1998. The Irish B-WIM system was installed near Aleån, 20 km south of the city of Luleå, on the E4 route (Figure 8.18(b)). Traffic is carried by one lane in each direction with no central median. The speed limit for heavy vehicles is 80 km/h.

The B-WIM system only participated in the test periods of June 1997, March 1998 (Figure 8.19) and June 1998. The records of the first two periods were acquired with a 4 Hz hardware low-pass filter. Hallström (1999) emphasises B-WIM as a promising technology for cold climates. Accuracy of B-WIM systems is not as influenced by the fast deterioration of the road surface as road WIM sensors.



(a) General location



(b) Detailed map

Figure 8.18 – Bridge Location (Luleå)



Figure 8.19 - Side View of Luleå Bridge

8.3.1 Installation

The installation carried out by the author in March 1998 is described. The bridge is a two span integral bridge with two equal spans of 14.6 m and is straight in plan (Figure 8.20). The bridge deck has a mid-span depth of 550 mm and is solid in cross-section.

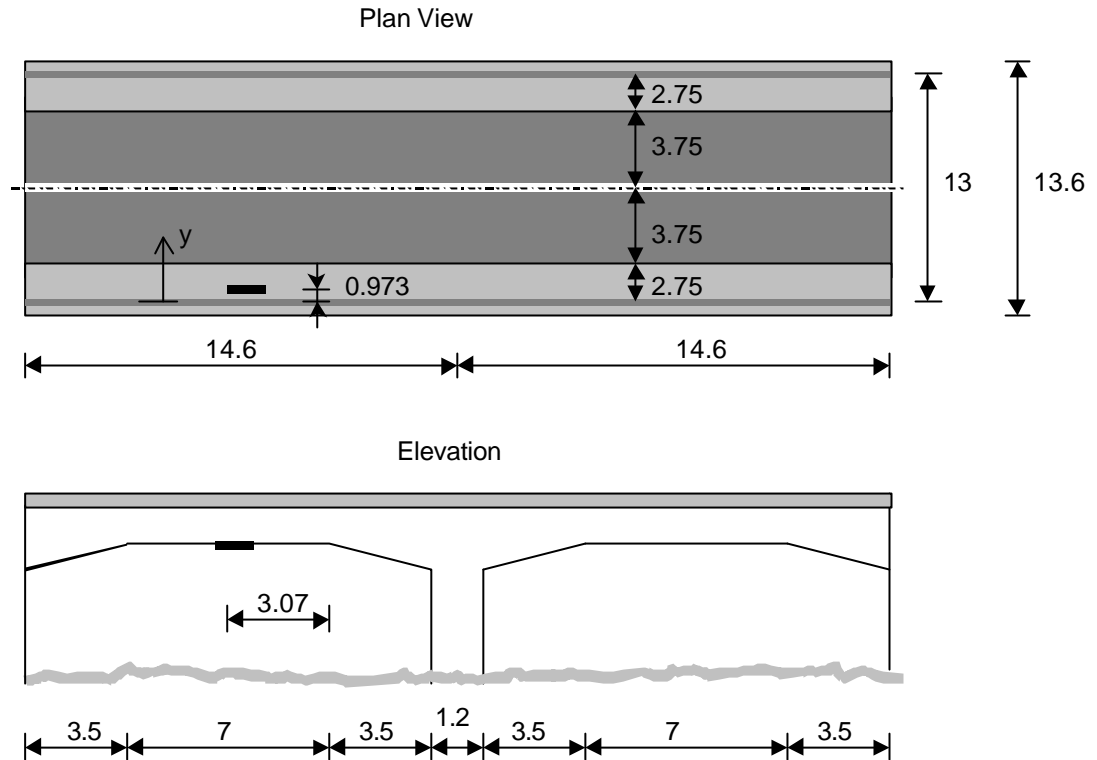


Figure 8.20 – Bridge layout (Luleå)

Mechanical strain amplifiers

Strain sensors were placed at the middle of the first span as represented in Figure 8.19. Eight mechanical strain amplifiers were bolted to the soffit of the bridge under the southbound carriageway of the first span (Figure 8.21). Cable connectors were placed on each of the cables, as these ones had to be removed for safety purposes at the end of each day's testing. In this way, mechanical strain amplifiers could be left on site for the duration of the test.

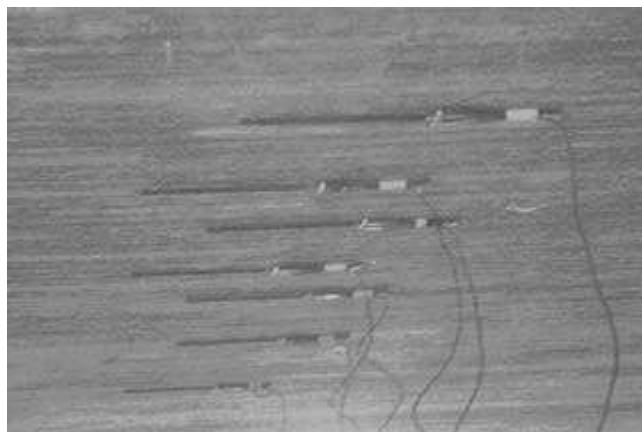


Figure 8.21 – Mechanical strain amplifiers (Luleå)

Table 8.10 gives the transverse position of the mechanical strain amplifiers, where transverse axis y is defined in Figure 8.20. Longitudinally, the amplifiers are about 7.17 m from the middle of the central column.

Table 8.10 - Distances of mechanical amplifiers (Luleå)

Mechanical strain amplifier no.	y (m)	Lane
1	0.973	Hard Shoulder
2	2.156	Hard Shoulder
3	2.973	Test lane
4	3.977	Test lane
5	4.97	Test lane
6	6.01	Test lane
7	7.507	Northbound lane
8	9.016	Northbound lane

Axle Detectors

Four pneumatic tubes were fixed across both lanes: one just before the bridge (at 15.70 m from the centre of the column between both spans), two immediately at the end of the first span (over the middle of the central column) and one after the bridge (Figure 8.22(a)). These tubes were fixed at the road edges with clamps. The pneumatic tubes were connected to the pneumatic converters in the middle of the bridge to minimise the lengths of tube required. These converters were inside a car to prevent them from freezing. The pneumatic converters and signal cables from the mechanical strain amplifiers were connected to the computer data acquisition equipment which was kept in the car (Figure 8.22(b)). The sampling rate for all channels was 250 Hz.



(a) Rubber tubes



(b) Data Acquisition Equipment

Figure 8.22 – Measuring Devices (Luleå)

8.3.2 Testing

A 3-axle truck with a rear tandem (static axle weights: 6.25, 8 and 6.5 tonnes, with axle spacings: 4.20 and 1.30 m) and a 6-axle semi-trailer with a rear tridem (axle weights: 7.3, 10.95, 8.5, 7.8, 8.1 and 7.95 tonnes, with axle spacings 4.20, 1.35, 5.35, 1.35 and 1.35 m) were used to evaluate B-WIM accuracy. The axle loads of these calibration trucks were measured with portable static scales. The data used for the analysis belongs to the test period of June 1997.

Bridge dynamics were found to be negligible. A record of the unfiltered free vibration of the bridge due to a fully laden 6-axle truck is shown in Figure 8.23. There are not significant vibrations remaining once the truck has left the second span of the bridge.

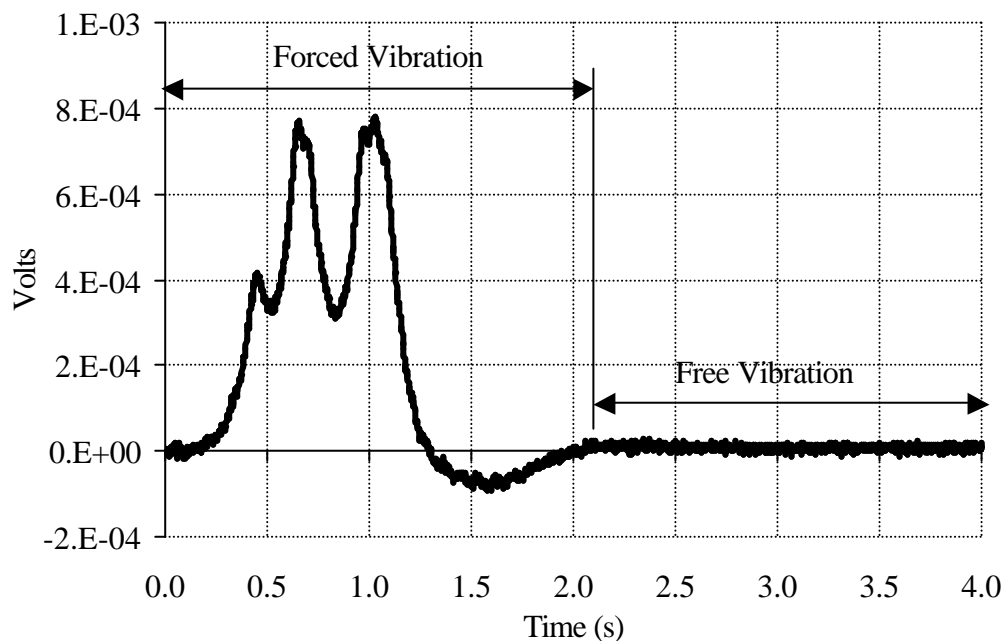
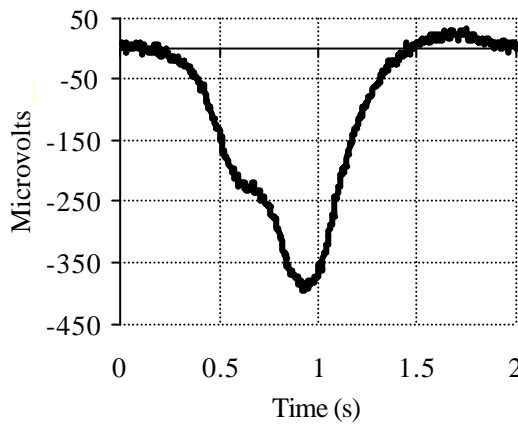


Figure 8.23 – Measured Record in Free Vibration (Luleå)

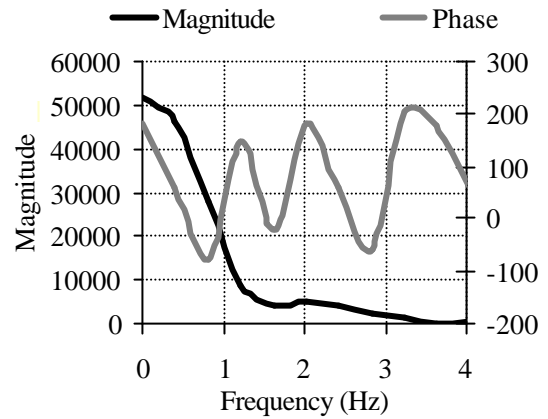
The determination of the influence line in this structure has been a tedious task, as the bridge behaviour appears to change for the different seasons where the test took place (Jacob et al 2000, McNulty 1999). These methods work in the time domain and they take a theoretical influence line as an initial starting point. However, the structural behaviour of this influence line could differ significantly from the bridge and the calculation of the ‘real’ influence line from experimental data can consume a considerable amount of time. These

difficulties are easily overcome by applying the calibration algorithm in the frequency domain suggested in Section 8.2. With this approach, the determination of boundary conditions is straightforward.

Figures 8.24(a) and (b) show the voltage-time history and the corresponding Fourier transform respectively, for the passing of a three-axle truck at 51.48 km/h.



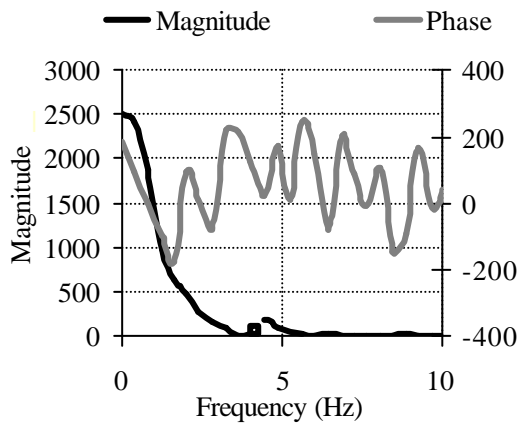
(a) Time domain



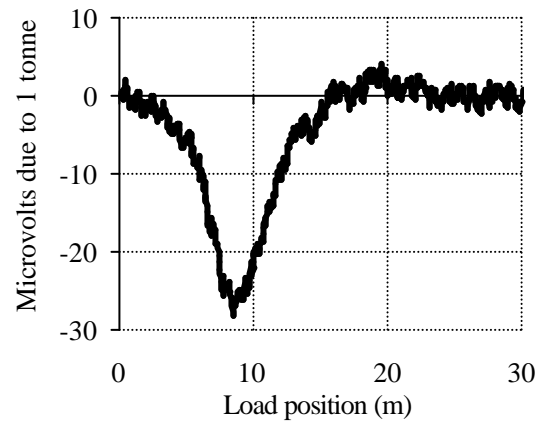
(b) Frequency domain

Figure 8.24 – Strain due to three-axle truck at 51.48 km/h (Luleå)

Figures 8.25(a) and (b) show the transform and inverse transform respectively when applying Equations 8.1 and 8.2 to the spectrum represented in Figure 8.24(b). Figure 8.25(b) represents the experimental influence line for this particular run.



(a) Frequency domain



(b) Influence line

Figure 8.25 – Bridge response due to a unit load (Luleå)

Accuracy analysis is done under limited reproducibility conditions (R1): two vehicles passing several times at different combinations of speed and with small variations in lateral position. The influence line from Figure 8.25(b) has been used for testing all runs, but a better approximation of the real influence line could have been obtained by averaging the experimental influence lines obtained for every calibration run. Table 8.11 shows the final result. Gross weight is not very accurate mainly due to the 4 Hz hardware filter. This filter smoothed out strain peaks and removed a significant static component from the total strain. The degree of accuracy achieved by other calibration methods based on adjustments in the time domain is one class better (Sections 3.5 and 3.7.4). However, these methods used a bigger number of runs for the same two calibration vehicles, but specially, two different influence lines depending on the vehicle speed.

Table 8.11 – Accuracy classification (Luleå) (R1)

(**n**: Total number of vehicles; **m**: mean; **s**: Standard deviation; **p₀**: level of confidence; **d**: tolerance of the retained accuracy class; **d_{min}**: minimum width of the confidence interval for π_0 ; **p**: Level of confidence of the interval $[-\delta, \delta]$)

Criterion	Relative error statistics				Accuracy calculation				Class Retained
	n	m (%)	s (%)	p ₀ (%)	Class	d (%)	d _{min} (%)	p (%)	
Single axle	23	-2.83	10.66	91.5	D+(20)	25	24.4	92.3	E(50)
Axle of group	76	0.30	26.83	94.6	E(50)	65	58.6	96.9	
Group of axles	33	0.16	9.99	92.8	D+(20)	23	22.1	94.0	
Gross Weight	23	0.45	6.62	91.5	C(15)	15	14.8	91.9	

Strain responses are plotted versus vehicle position on the bridge in Figure 8.26. Significant differences in magnitude can be seen depending on the two ranges of speed (about 50 km/h and 80 km/h) and the truck configuration (three- or six-axle truck). Filtering is the main cause of this phenomenon. The bridge response due to the three-axle truck is smaller at 80 km/h than at 50 km/h as shown in Figure 8.26(a), unlike the response due to the six-axle truck which is smaller at 50 km/h.

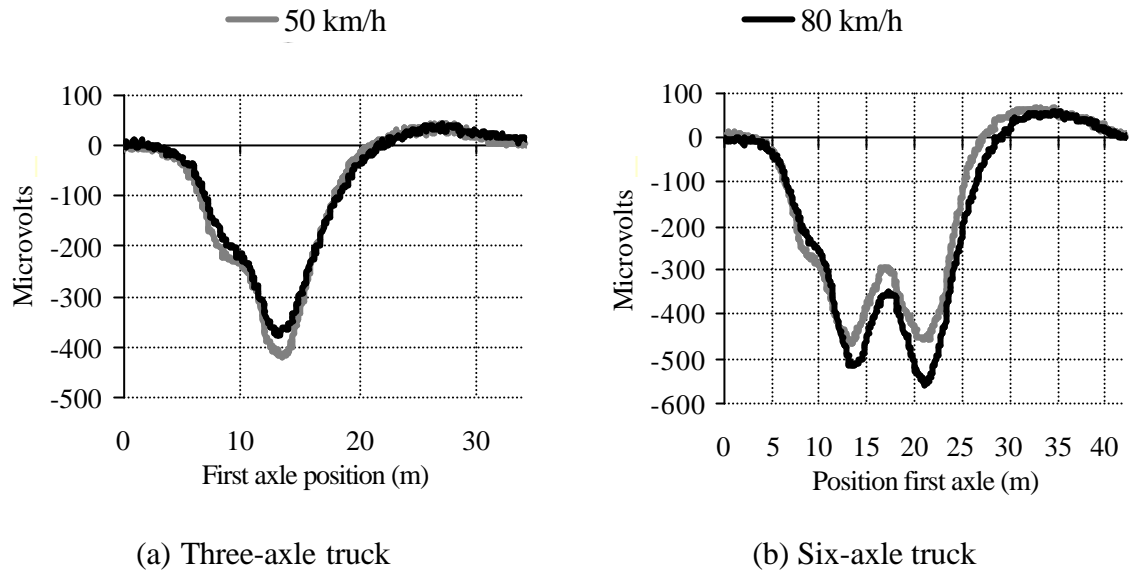


Figure 8.26 – Influence of 4Hz hardware filter on the record (Luleå)

If the test took place in full repeatability conditions (several passes of one vehicle at the same speed and with the same load) for the three-axle truck travelling at about 50 km/h, the accuracy classes that result are given in Table 8.12. The improvement in prediction of single axle weights is noteworthy (from D+(20) to B+(7)), but the GVW and axle group criteria remain in class C(15) and D+(20) respectively.

Table 8.12 – Accuracy classification (Luleå) (r1) (3-axle truck at 50 km/h)

(**n**: Total number of vehicles; **m**: mean; **s**: Standard deviation; **p₀**: level of confidence; **d**: tolerance of the retained accuracy class; **d_{min}**: minimum width of the confidence interval for π_0 ; **p**: Level of confidence of the interval $[-\delta, \delta]$)

Criterion	Relative error statistics				Accuracy calculation				Class Retained
	n	m (%)	s (%)	p ₀ (%)	Class	d (%)	d _{min} (%)	p (%)	
Single axle	8	-0.30	3.22	93.4	B+(7)	11	9.7	96.2	E(30)
Axle of group	16	-0.16	12.51	96.8	E(30)	41	36.2	98.5	
Group of axles	8	0.30	6.29	93.4	D+(20)	23	19.0	97.4	
Gross Weight	8	0.12	3.62	93.4	C(15)	15	10.9	98.7	

If the runs of the six-axle truck at 50 km/h are included in the testing, all accuracy classes are worse as shown in Table 8.13. This is motivated by the different smoothing effect of the hardware filter in different axle group configurations. The influence line in Figure 8.25(b) works best for that three-axle configuration, but it changes for other trucks. Axle of

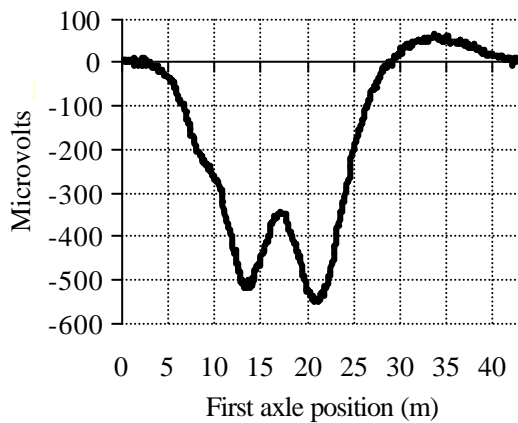
group and group of axles criteria are the ones determining the overall accuracy class again. The mean error for the axle group is negative, this is, the axle group is being underweighed as a result of the loss of static component caused by filtering.

Table 8.13 – Accuracy classification (Luleå) (R1) (3 and 6-axle trucks at 50 km/h)

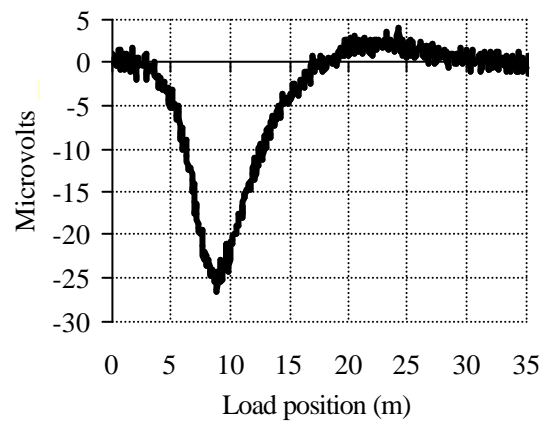
(**n**: Total number of vehicles; **m**: mean; **s**: Standard deviation; **p₀**: level of confidence; **d**: tolerance of the retained accuracy class; **d_{min}**: minimum width of the confidence interval for π_0 ; **p**: Level of confidence of the interval $[-\delta, \delta]$)

Criterion	Relative error statistics				Accuracy calculation				Class Retained
	n	m (%)	s (%)	p ₀ (%)	Class	d (%)	d _{min} (%)	p (%)	
Single axle	13	7.07	4.11	87.9	B(10)	15	14.6	89.5	E(60)
Axle of group	41	-4.45	30.81	93.4	E(60)	77	68.6	96.3	
Group of axles	18	-3.44	11.38	90.3	D(25)	28	26.4	92.4	
Gross Weight	13	0.74	8.72	87.9	D+(20)	20	19.9	88.2	

If the calibration took place for the six-axle truck travelling at about 80 km/h, the results are shown in Figure 8.27. Compared to the influence line derived at 50 km/h (Figure 8.25(b)), the influence line at 80 km/h is very similar in the first span, but lightly bigger and smoother in the second span.



(a) Measured record



(b) Experimental Influence line

Figure 8.27 – Calibration of 6-axle truck at 80 km/h

The accuracy classes in full repeatability conditions for runs of the six-axle truck at 80 km/h are given in Table 8.14. There is a significant improvement in all accuracy classes derived from the lower deviation in each of the single runs.

Table 8.14 – Accuracy classification (Luleå) (r1) (6-axle truck at 80 km/h)

(**n**: Total number of vehicles; **m**: mean; **s**: Standard deviation; **p₀**: level of confidence; **d**: tolerance of the retained accuracy class; **d_{min}**: minimum width of the confidence interval for π_0 ; **p**: Level of confidence of the interval $[-\delta, \delta]$)

Criterion	Relative error statistics				Accuracy calculation				Class Retained
	n	m (%)	s (%)	p ₀ (%)	Class	d (%)	d _{min} (%)	p (%)	
Single axle	5	2.61	0.91	84.8	A(5)	8	4.8	99.5	D+(20)
Axle of group	25	-0.10	9.52	97.6	D+(20)	30	26.9	98.9	
Group of axles	10	-0.40	1.62	95.0	A(5)	7.14	4.9	99.5	
Gross Weight	5	0.02	1.51	84.8	A(5)	5	4.5	89.4	

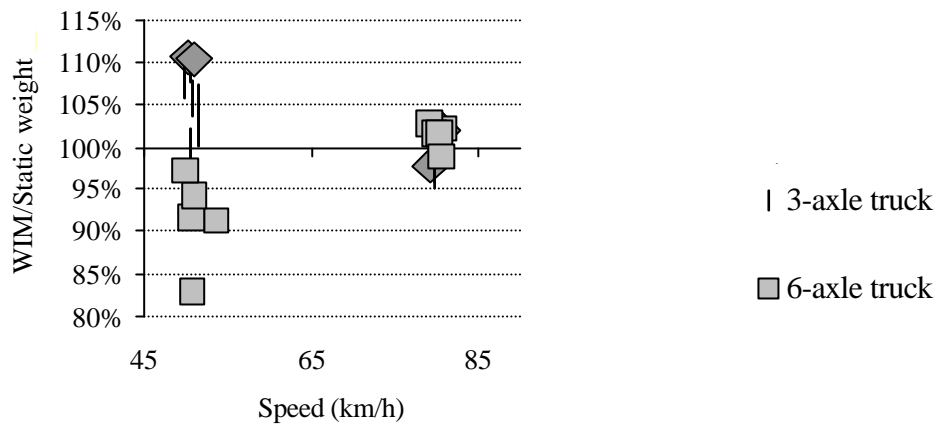
In Table 8.15, the runs of the three-axle and six-axle trucks at 80 km/h are included in the analysis (Limited reproducibility conditions) and the overall accuracy improves from D+(20) to C(15).

Table 8.15 – Accuracy classification (Luleå) (3 and 6-axle trucks at 80 km/h) (R1)

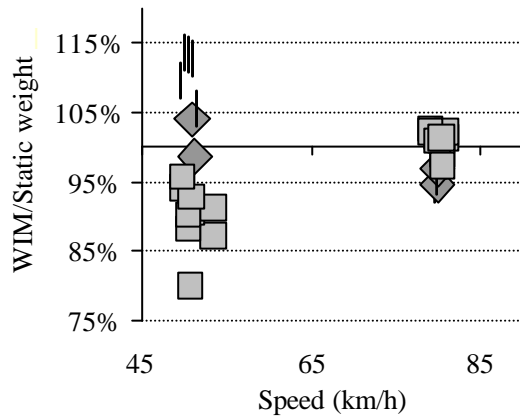
(**n**: Total number of vehicles; **m**: mean; **s**: Standard deviation; **p₀**: level of confidence; **d**: tolerance of the retained accuracy class; **d_{min}**: minimum width of the confidence interval for π_0 ; **p**: Level of confidence of the interval $[-\delta, \delta]$)

Criterion	Relative error statistics				Accuracy calculation				Class Retained
	n	m (%)	s (%)	p ₀ (%)	Class	d (%)	d _{min} (%)	p (%)	
Single axle	10	4.48	3.13	85.0	B+(7)	11	10.2	89.2	C(15)
Axle of group	35	-0.51	11.16	93.0	C(15)	25	24.7	93.3	
Group of axles	15	-0.70	2.85	89.1	A(5)	7.14	6.6	92.3	
Gross Weight	10	0.04	2.13	85.0	A(5)	5	4.9	86.3	

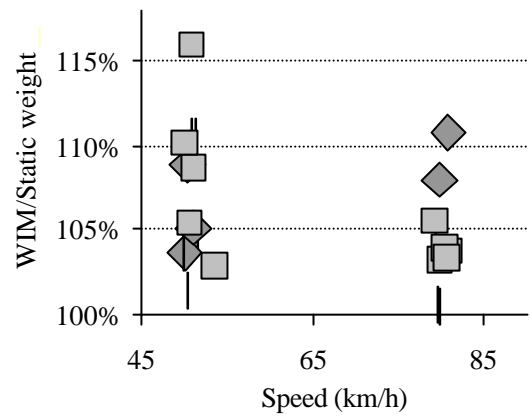
Figure 8.28 illustrates the errors in predicted axle weights using two influence lines (at 50 and 80 km/h). At 50 km/h, errors are bigger due to a higher deviation in the strain response.



(a) Gross weight



(b) Axle group



(c) Single axle

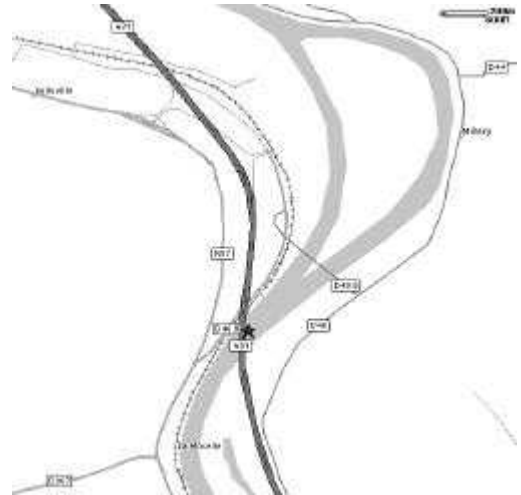
Figure 8.28 – Errors in weights by using a theoretical beam model

8.4 BELLEVILLE, TWO SPAN (50 m EACH) CONTINUOUS BRIDGE

The Belleville site is located on the southbound carriageway of the A31 Motorway between Metz and Nancy in North Eastern France. Data was obtained in June 1998 as part of the Continental Motorway Test. The location of the Belleville B-WIM site is marked in Figure 8.29.



(a) General location



(b) Detailed map

Figure 8.29 – Bridge Location (Belleville)

The bridge is a two span composite box girder, consisting of a steel box with a concrete deck (Figure 8.30). The spans are 54.89 and 51.69 m long. There are two lanes of traffic crossing this bridge in the same direction. The speed limit on this section of the road is 130 km/h for cars and 90 km/h for heavy vehicles.



Figure 8.30 – Side View of Belleville Bridge

8.4.1 Installation

The installation of axle detectors, data acquisition equipment and strain gauges is described below.

Axle Detectors

Low-grade piezoelectric axle detectors were permanently embedded into the pavement to record the occurrences of axles in both lanes of traffic. These sensors, together with associated hardware, result in a 20 ms voltage output pulse being transmitted when an axle strikes a sensor. The sensors are located 10.25 m prior to the bridge (Figure 8.31(a)). The installation of these sensors required road closure in dry weather conditions. The coaxial cables from the piezos were connected to the SCXI through an interface as described in Section 4.3.1. There were a lot of difficulties with the signals from the piezo sensors, and some axles were still passing undetected at the time of the test.

In the same experiment, Lutzenberger and Baumgärtner (2000) from the Technische Universität München (TUM) demonstrated how axle and lane identification can be possible from measuring the longitudinal bending of the concrete slab. Records from two locations spaced longitudinally by a fixed amount allow for calculation of speed and axle spacings (Section 4.3.2). They also discuss the influence of road roughness (measured by LCPC) on the bridge and truck response.

Data acquisition equipment

The SCXI data acquisition equipment was placed within the box section of the bridge for safe dry storage (Figure 8.31(b)). The equipment was located at midspan to keep the length of the strain gauge cables and the distance to the piezoelectric sensors relatively short. Electricity is available within the bridge. Strain gauges are connected to the SCXI through a four core high quality shielded cable.



(a) Piezos



(b) Data Acquisition Equipment

Figure 8.31 – Data Collection Devices (Belleville)

Strain gauges

Strain gauges (120 Ω and 2.13 gauge factor) were attached at a number of longitudinal locations along the bridge to test a multiple-sensor BWIM system. Each span is divided into eight sections separated by diaphragm walls as shown in Figure 8.32. Five longitudinal positions were chosen for strain gauge installation. These positions are midspan and three quarter span of the north span, over the central support, and one quarter and midspan of the south span (Figure 8.32).

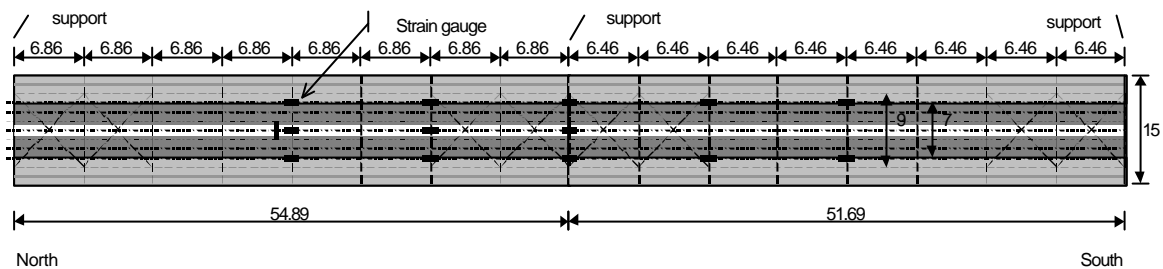


Figure 8.32 – Layout of Belleville Bridge

Seven stiffeners in the longitudinal direction are attached to the soffit plate of the steel box. Additional stiffeners are located in the areas of the bridge close to the central support. The longitudinal bending of two or three vertical stiffeners is measured at each instrumented section as illustrated in Figure 8.33.

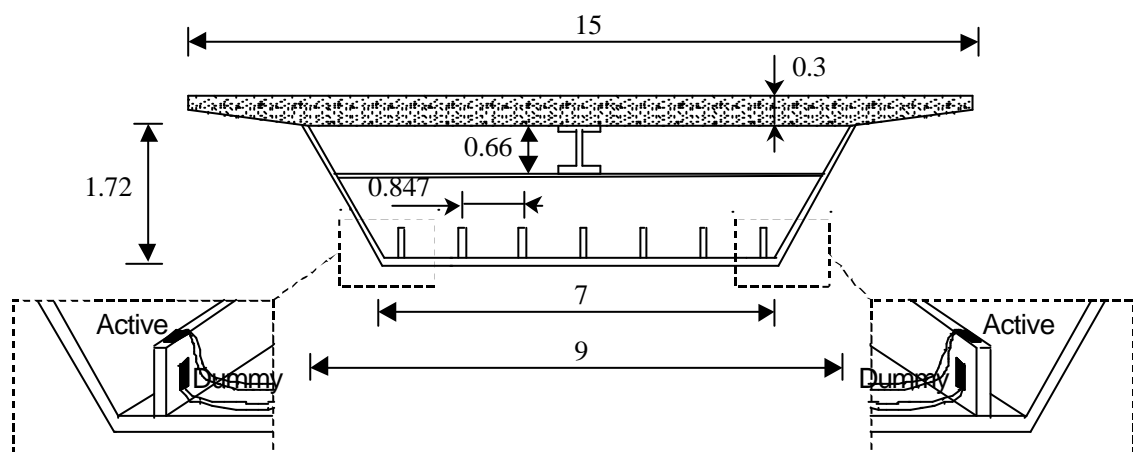


Figure 8.33 – Cross Section and Strain Gauge Location

The protective paint coating of the stiffeners is removed to glue the gauges directly to the bare steel. Each pair of gauges is arranged in a half bridge configuration with one active and one dummy gauge (Section 4.2.1). Originally, strain gauges were installed by the Centre d'Etudes Techniques de l'Equipment de l'est (CETÉ de L'EST) at the two outer stiffeners at 4 longitudinal locations (total of 8 sensor locations). Due to the lack of resolution (Kealy 1997), the author placed more gauges at the central stiffener in three of the four instrumented sections and two sensors in a new section at the middle of the second span. The position of all 13 locations is given in Table 8.16.

Table 8.16 - Distances of strain gauges from support (Belleville)

Sensor location no.	Stiffener No.	Longitudinal position (m)	Sensor location no.	Stiffener No.	Longitudinal position (m)
1	1	27.39	7	1	54.94
2	4	27.39	8	4	54.94
3	7	27.39	9	7	54.94
4	1	41.12	10	1	67.76
5	4	41.12	11	7	67.76
6	7	41.12	12	1	80.69
			13	7	80.69

Unfortunately, as a result of isolation problems and electrical interference, the data obtained at the tests was not usable. The strain measurements carried out by the TUM team at the middle of the north span are used for the accuracy analysis that follows.

8.4.2 Testing

The dynamic properties of the bridge were derived from measured strains and accelerations by Lutzenberger and Baumgärtner (1999). They used this data to design a finite element model of the bridge in correspondence with the real frequencies. Kessler (1997) refined this model and the modes of vibration are represented in Figure 8.34.

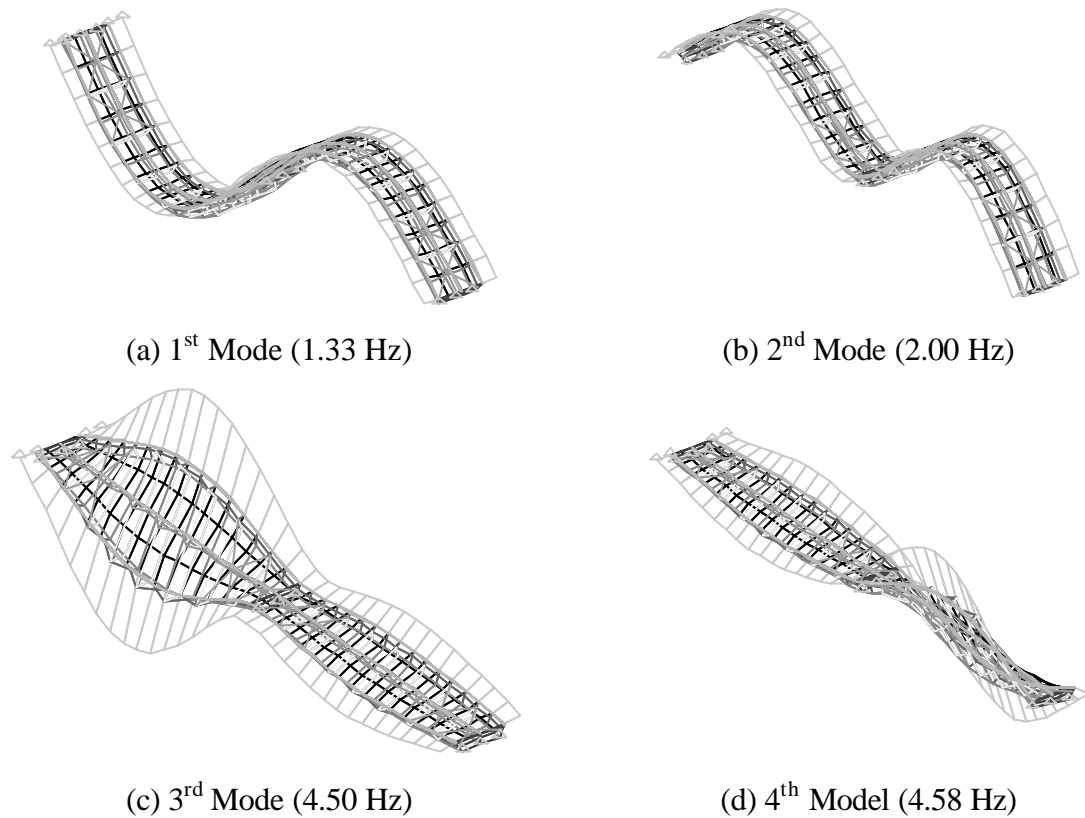


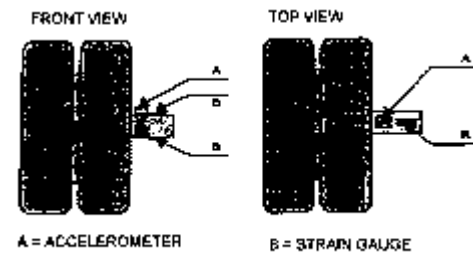
Figure 8.34 - Modes of Vibration of Belleville Bridge

An instrumented vehicle was used during the test. VTH (Finland) provided the data on the dynamic wheel loads applied by the truck. The vehicle is a three axle rigid lorry with axle spacings of 4.20 m and 1.20 m (Figure 8.35(a)). Static axle weights are 58.74, 86.19 and 72.17 kN for the first, second and third axles respectively. A theoretical model of this vehicle has been presented in Section 6.4. All axles are equipped with traditional steel springs. The tandem has dual tyres and all tyres have a diameter of 1.05 m.

Dynamic wheel loads are measured through strain gauges and accelerometers installed on the axles as shown in Figure 8.35(b). Strain gauges measure bending moment of the axle while accelerometers measure the inertial force component. The wheel load applied to the pavement is derived from the bending moment measured by the strain gauges plus the mass outboard of the strain gauges multiplied by the vertical acceleration given by the accelerometers.



(a) VTH truck



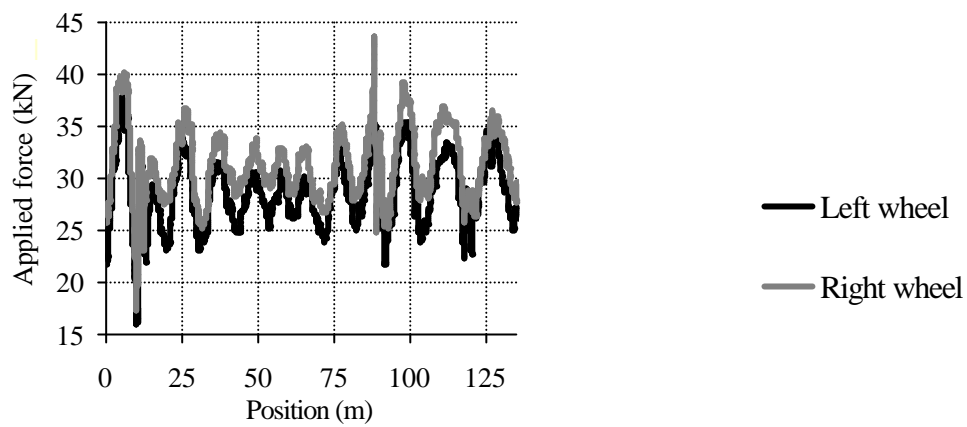
(b) The locations of the sensors on the axle of vehicle

Figure 8.35 – Instrumented vehicle (after Huhtala et al. 1998)

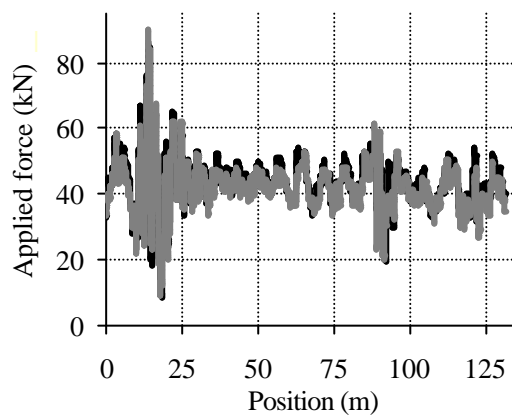
Dynamic wheel load measurements are related to the road section under study using an electric eye to detect reflective tapes glued across the road lane every 10 m. There are a total of 13 strips with the first strip placed 10 m before the bridge joint (just 0.25 m after the second piezo to synchronise recordings of the B-WIM system and truck). The sampling rate is 1000 Hz. A total of six crossings took place at about 80 km/h.

Figure 8.36 shows the wheel forces applied by each axle for one of the runs. There are high dynamic forces prior to the bridge (from 1 to 10 m in Figure 8.36) and at the joint (located at 10 m) due to the unevenness of the road profile. These forces will cause strong bridge vibrations. The wheels of the rear tandem have a dynamic amplification of about 100% at the joint (Figures 8.36(b) and (c)). The forces at the end of the bridge are not as important as the road is relatively smooth along the bridge, except at about 90 m. This is due to a portable WIM system mounted on the road surface that caused wheels to jump and dynamic forces to increase by a maximum of 80% in the right wheel of the third axle (Figure 8.36(c)). There are also small differences between the left and right wheels of an axle caused by the difference in irregularities of each path.

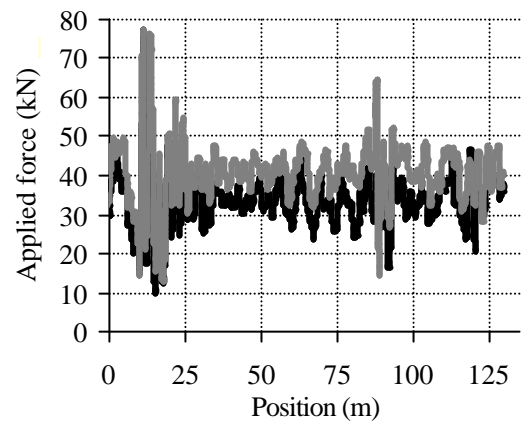
The spectra of dynamic wheel forces are represented in Figure 8.37. There are dominant frequencies of 2.3 Hz for the front axle (body bounce) and 2.3 Hz and 9 Hz (axle vibrations) for the rear tandem.



(a) First axle

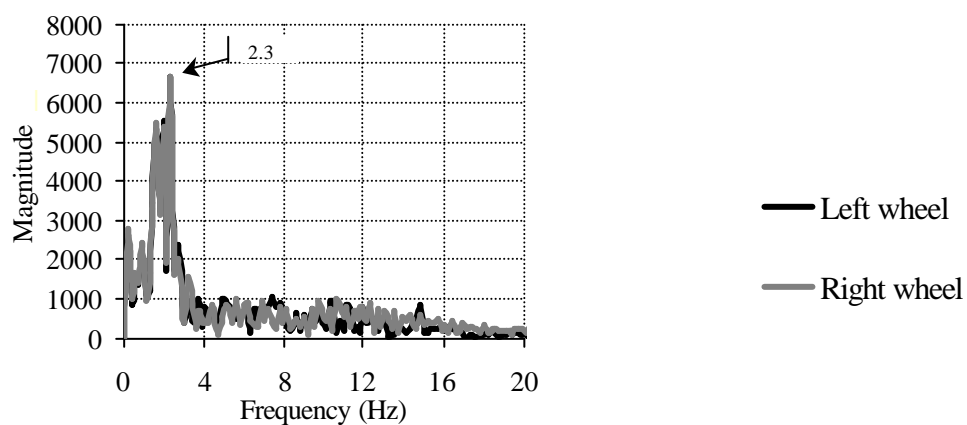


(b) Second axle



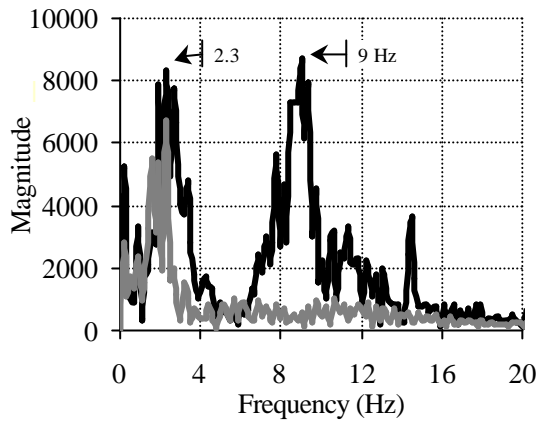
(c) Third axle

Figure 8.36 – Dynamic wheel forces

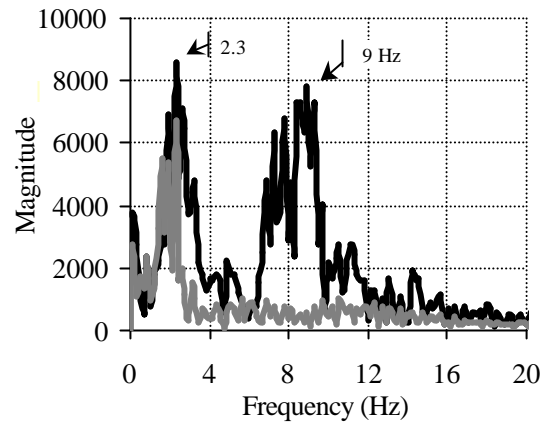


(a) First axle

Figure 8.37 (continued on following page)



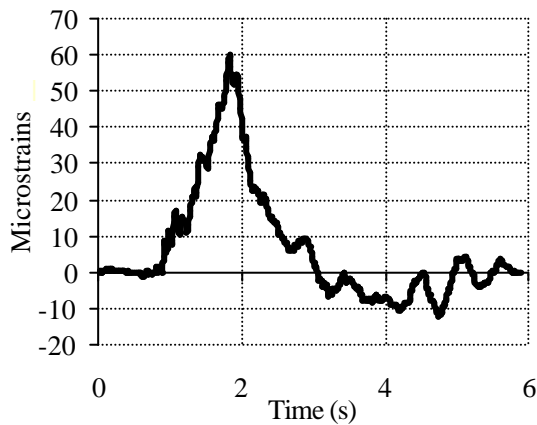
(b) Second axle



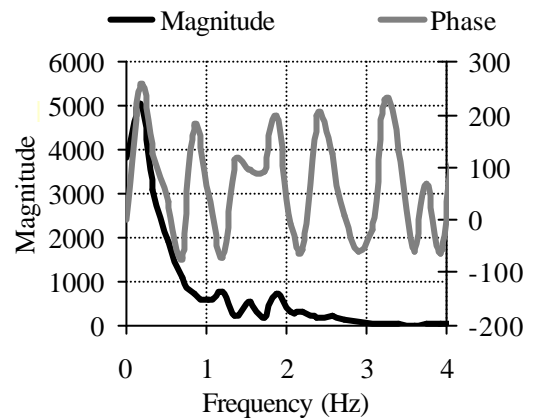
(c) Third axle

Figure 8.37 – Spectra of Dynamic wheel forces

The B-WIM system was calibrated following the experimental procedure described in previous sections. The measured record and its spectra are given in Figure 8.38.



(a) Time Domain



(b) Frequency Domain

Figure 8.38 – Measurements of 3-axle truck at 82.74 km/h (Belleville)

The results of calibration are shown in Figure 8.39.

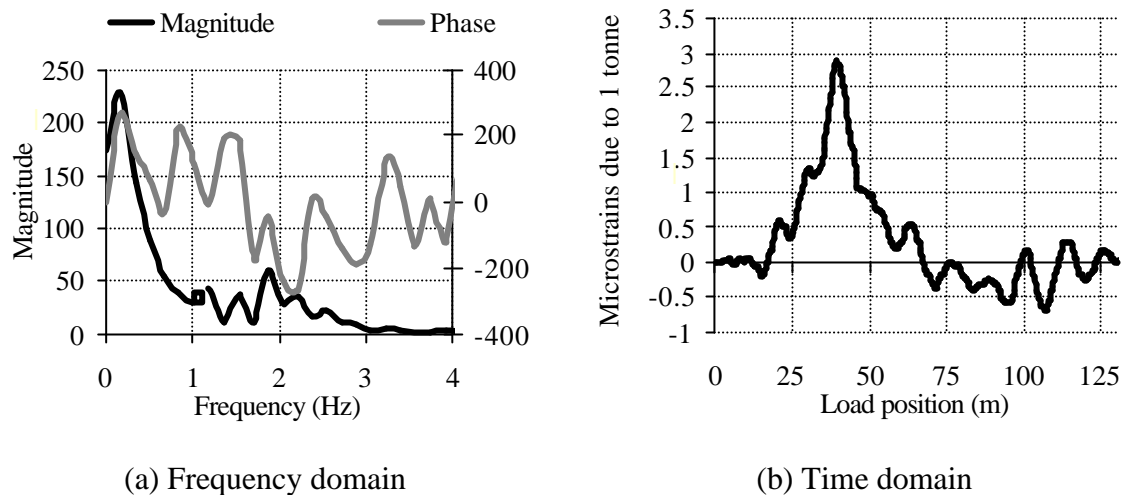


Figure 8.39 – Bridge response due to a unit load travelling at 82.74 km/h (Belleville)

The six runs of the VTT truck are analysed in full repeatability conditions (r1) in Table 8.17 by a dynamic algorithm developed by the author. The total unit response due to a load at 82.74 km/h is used directly for all runs. Unlike an influence line, this unit response will be different for other speeds. The algorithm uses the measurements of the longitudinal bending of the steel girder and steel box at midspan. A class B(10) is achieved for gross weight, but the vehicles acts as a whole and individual axle weights can not be predicted.

Table 8.17 – Accuracy classification by dynamic algorithm (r1) (Belleville)

(**n**: Total number of vehicles; **m**: mean; **s**: Standard deviation; **p₀**: level of confidence; **d**: tolerance of the retained accuracy class; **d_{min}**: minimum width of the confidence interval for π_0 ; **p**: Level of confidence of the interval $[-\delta, \delta]$)

Criterion	Relative error statistics				Accuracy calculation				Class Retained
	n	m (%)	s (%)	p ₀ (%)	Class	d (%)	d _{min} (%)	p (%)	
Single axle	6	127.9	49.94	89.6	E(250)	300	252.8	96.9	E(250)
Group of axles	6	-47.3	22.14	89.6	E(100)	110	102.8	93.1	
Gross Weight	6	0.06	2.70	89.6	B(10)	10	8.2	95.4	

It was thought that the response of transverse bending might be more sensitive to individual axles. The total response due to a unit moving load is calculated for the transverse bending of the concrete slab. Figures 8.40(a) and (b) show the measured record for the fifth run of the calibration truck and the corresponding spectra.

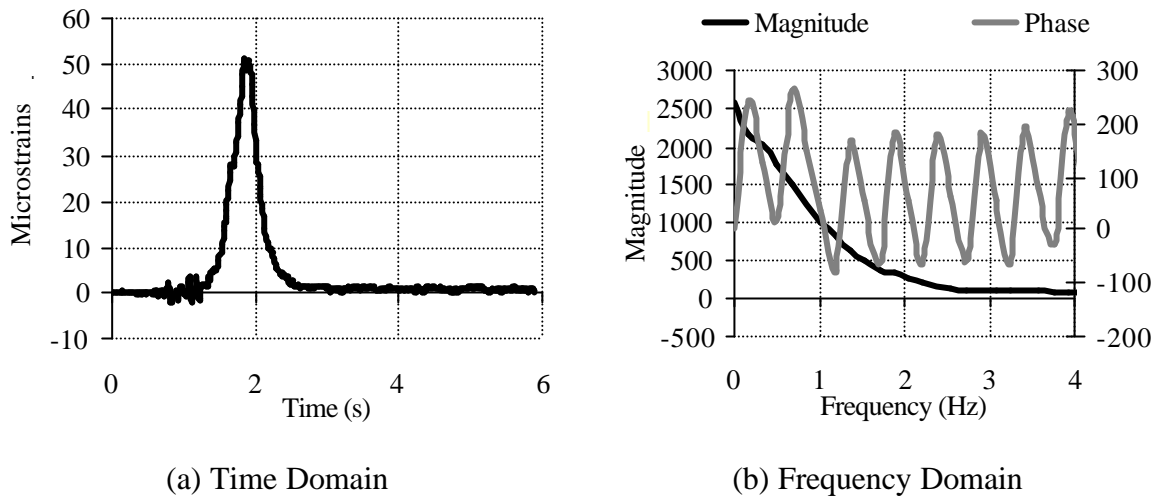


Figure 8.40 – Transverse bending at midspan due to truck at 82.74 km/h (Belleville)

The corresponding dynamic unit response in frequency and time domains is given in Figures 8.41(a) and (b) respectively.

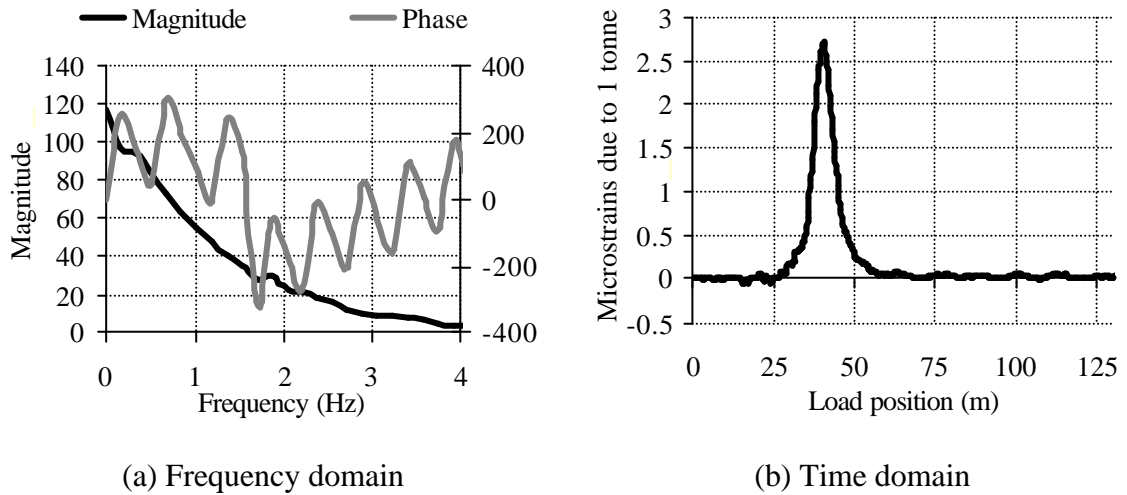


Figure 8.41 – Transverse bending due to a unit load travelling at 82.74 km/h (Belleville)

Table 8.18 gives the accuracy classes achieved by a dynamic algorithm based on this transverse bending of the concrete slab. Accuracy in GVW decreases when considering transverse bending instead of longitudinal bending. Transverse bending is a very localised effect that can be isolated from other vehicles in the bridge (the shape of the unit response is narrower), but it is very sensitive to transverse position of the truck on the bridge. In a one-dimensional B-WIM algorithm, transverse location can not be managed and the result in GVW is very poor.

Table 8.18 – Accuracy classification by dynamic algorithm (transverse) (r1) (Belleville)

(**n**: Total number of vehicles; **m**: mean; **s**: Standard deviation; **p₀**: level of confidence; **d**: tolerance of the retained accuracy class; **d_{min}**: minimum width of the confidence interval for π_0 ; **p**: Level of confidence of the interval $[-\delta, \delta]$)

Criterion	Relative error statistics				Accuracy calculation				Class Retained
	n	m (%)	s (%)	p ₀ (%)	Class	d (%)	d _{min} (%)	p (%)	
Single axle	6	100.2	33.30	89.6	E(180)	216	183.4	97.0	E(180)
Group of axles	6	-35.64	16.91	89.6	E(75)	82.5	78.0	92.6	
Gross Weight	6	1.11	11.70	89.6	E(40)	40	35.6	93.5	

Figure 8.42 illustrates longitudinal and transverse bending for the six runs of the calibration truck. It can be seen how deviation in strain is higher for transverse bending, probably due to variations in lateral position (Strain peak is around 60 $\mu\epsilon$ for longitudinal bending in any run, but varies from 45 to 65 $\mu\epsilon$ for transverse bending). Transverse bending appears to be more adequate for weighing individual axles, but this requires a two-dimensional algorithm and more strain sensors to take into count the transverse position of the truck.

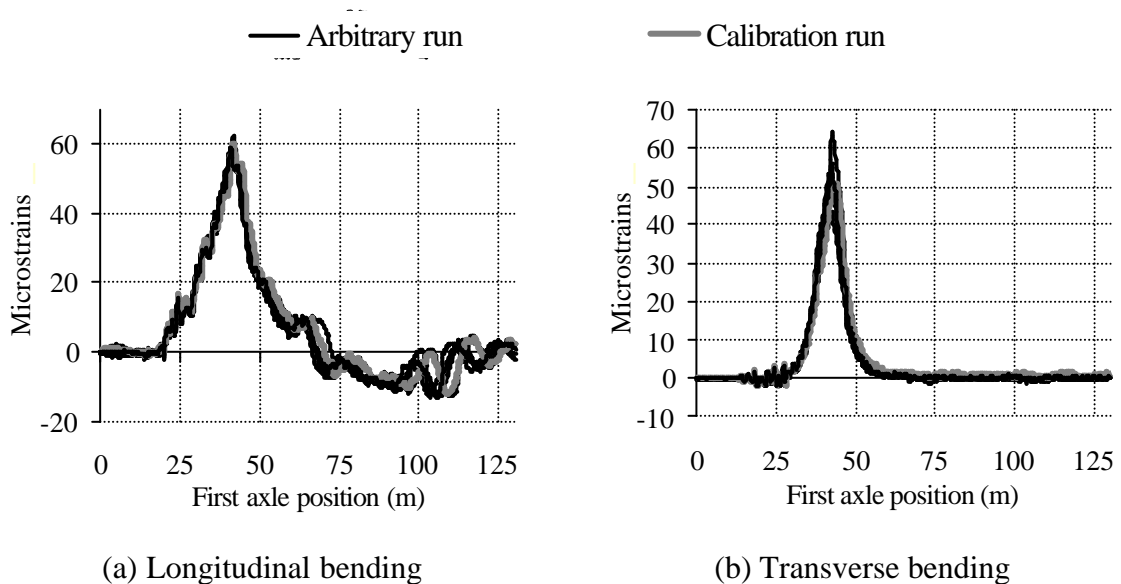


Figure 8.42 – Measured records at midspan due to three-axle truck (Belleville)

8.5 SLOVENIA, MEDIUM SPAN (32 m) SIMPLY SUPPORTED BRIDGE

The fourth site is located in Slovenia. The bridge is a 32 m long simply supported beam and slab. There are five beams along the underside of the bridge and the bridge has two lanes with traffic running in opposing directions. The instrumentation consisted of six longitudinal sections spaced every 4 m (see Figure 8.43). Two strain sensors were placed at each section, on the 2nd and 4th beam of the bridge. Data was recorded at 512 Hz.

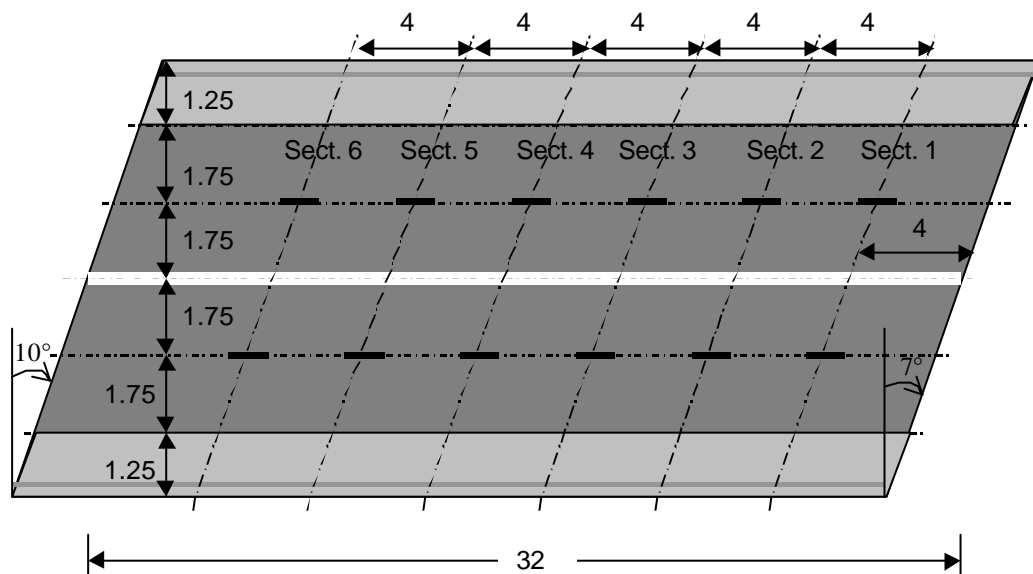


Figure 8.43 – Layout of Slovenian bridge

The dynamic multiple sensor algorithm (Section 7.5.2) is tested for each lane and direction of traffic flow separately. The signal from two sensors at the same section is added together for calculation purposes. This results in six equations (one per longitudinal section) at each instant.

8.5.1 Testing of the northbound carriageway

A two-axle truck with axle spacing of 4.35 m and static weights, 33.93 kN and 126.5 kN in the front and rear axles respectively, is driven over the bridge in the north-south direction at 59.85 km/h. Figure 8.44 shows the record in free vibration corresponding to two sensors at midspan. From this figure, a damped frequency of 3.54 Hz and 5% damping result. The

natural frequency is 3.54 Hz. These parameters have been obtained following the guidelines given in Section 5.2.1.

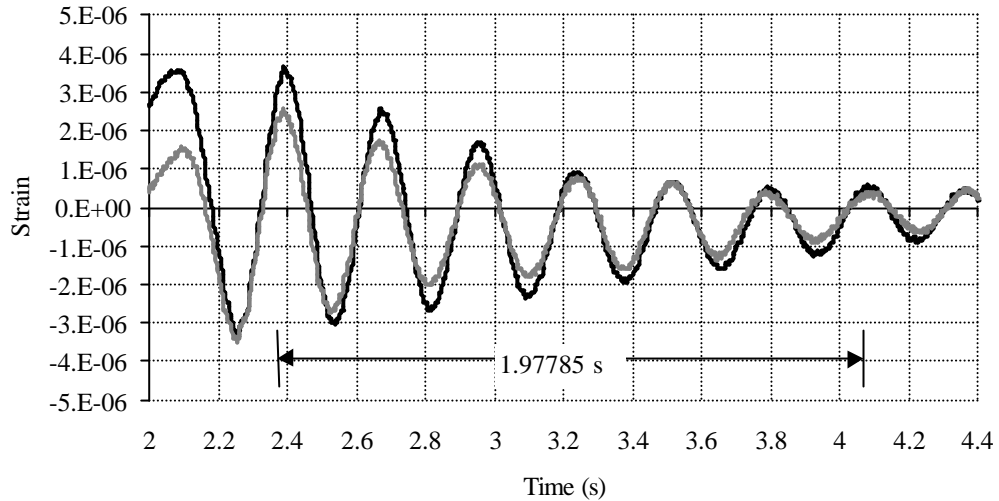


Figure 8.44 – Record in Free vibration (Slovenia)

The system is calibrated by obtaining the spectrum defined by Equations 8.1 and 8.2, and then by calculating the inverse Fourier transform. Measurement on site and dynamic response due to a unit moving load are represented in Figure 8.45 for longitudinal sections 1, 2 and 3 (Figure 8.43), and in Figure 8.46 for sections 4, 5 and 6. The origin of these curves is related to the instant the first axle hits the second axle detector, placed 3.15 m before the bridge joint. By using this reference at a safe distance from the influence of the bridge joint, there is no need to know at what exact position the applied load causes the bridge to start bending. In this way, the uncertainty on the real boundary conditions and the very small strains generally induced near the supports is avoided.

An additional advantage of this calibration method is that it allows for sensors of different sensitivity to be installed without any disturbance to the final results. Thus, a theoretical model of a simply supported bridge would be expected to generate bigger strains at midspan, but this calibration method is based on ‘sensors’, not structural models representing assumed bridge behaviour.

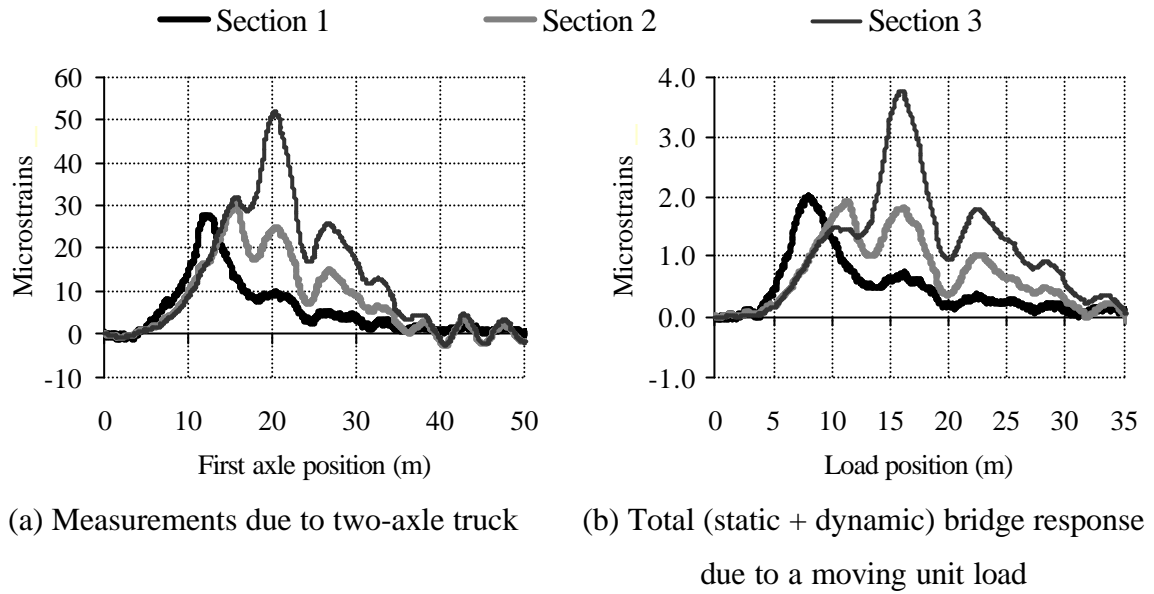


Figure 8.45 – Calibration of sections at 4, 8 and 12 m in northbound lane (Slovenia)

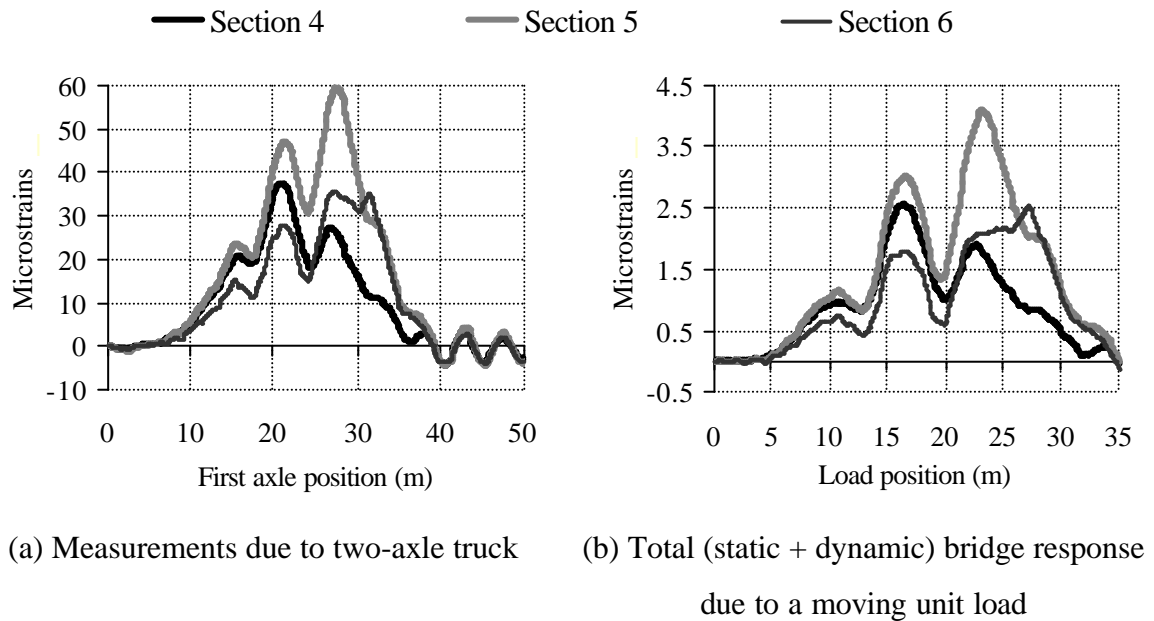


Figure 8.46 – Calibration of sections at 16, 20 and 24 m in northbound lane (Slovenia)

The influence lines obtained in Figures 8.45 and 8.46 are valid only for that speed if a dynamic multi-sensor algorithm is to be used. For other speeds that are not available from calibration; it will be necessary to interpolate from available responses calibrated at similar speeds or otherwise, to derive them from dynamic models. If an influence line is required, dynamics can be removed from this experimental calibration in one of several ways:

- (a) Filtering of the total response due to a single load: The risk of suppressing the static component has been reduced as the signal due to one single axle is to be filtered (there are no axle groups). Filtering can be safe if the first natural frequency of the bridge is high enough.
- (b) If the first natural frequency of the bridge is relatively low or the real influence line is likely to be very sharp, filtering could smooth out peaks containing part of the static response. In this case, dynamics could be removed through specific models of the bridge behaviour (i.e. Equation 5.31). Hints to obtain the parameters involved in these models are given in Section 9.2.
- (c) Another possibility to obtain the influence line is to use the calibration run corresponding to the lowest speed. The bridge response will be closer to the static as the vehicle speed approaches zero (Section 5.3).

The curves obtained in Figures 8.45(b) and 8.46(b) can be used to calculate axle force on a continuous basis as explained in Section 7.5.2 for the multiple-sensor algorithm. The results are shown in Figure 8.47.

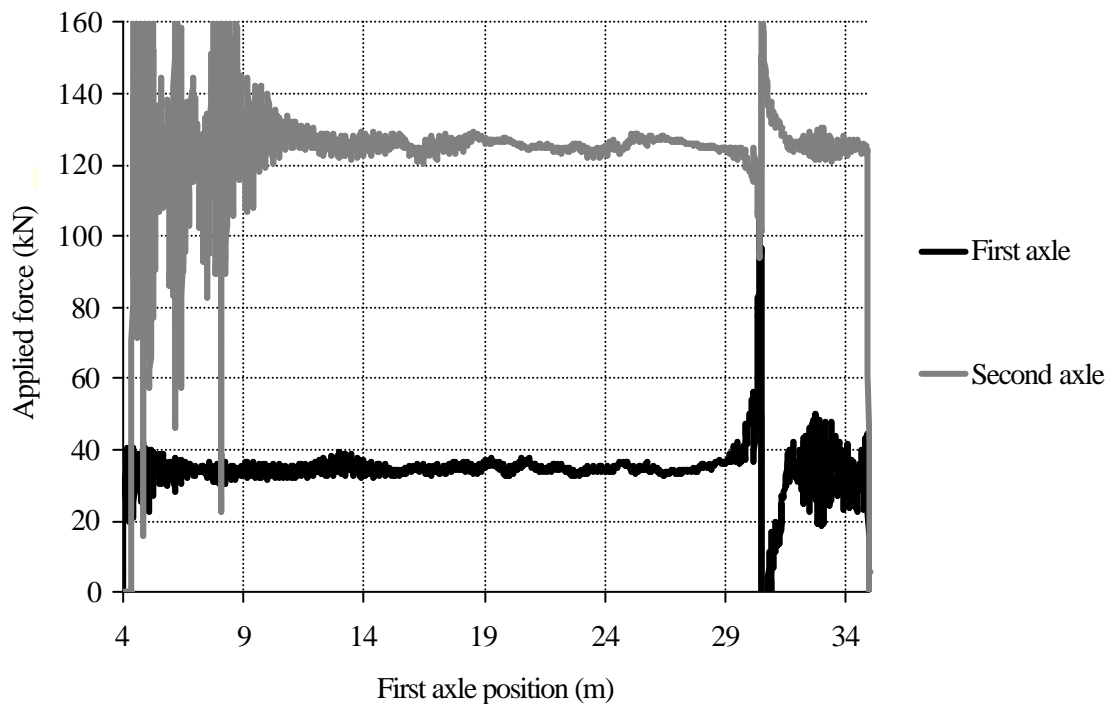


Figure 8.47 – Calculated load history in northbound carriageway (Slovenia)

The origin of the x -axis is related to the location of the second axle detector, 3.15 m before the bridge. Hence, instantaneous calculation of the second axle is only feasible after about 7.5 m, though strains are too small at this stage to validate results. According to this figure, a very good approximation of the static value (34 and 126.5 kN) can be obtained along most of the bridge (except when an axle enters or leaves the bridge due to rounding errors).

8.5.2 Testing of the southbound carriageway

A three axle truck with 3.22 and 1.37 m axle spacings, and 61.19 and 178.66 kN in the front axle and rear tandem respectively, was driven in the south-north direction at 57.56 km/h in the adjacent lane to the one tested in Section 8.5.1. The measurements for each section are shown in Figures 8.48(a) and 8.49(a). The bridge response due to a unit load travelling at 57.56 km/h for this carriageway and direction of flow is represented in Figures 8.48(b) and 8.49(b). The origin of the curves ($x = 0$) is related to the instant the first axle of the vehicle hits the second axle detector, placed 2.55 m before the bridge joint at the south end. Only the total weight of the tandem was available, so it was assumed for the calibration that the total weight of the tandem was evenly distributed between the two individual axles.

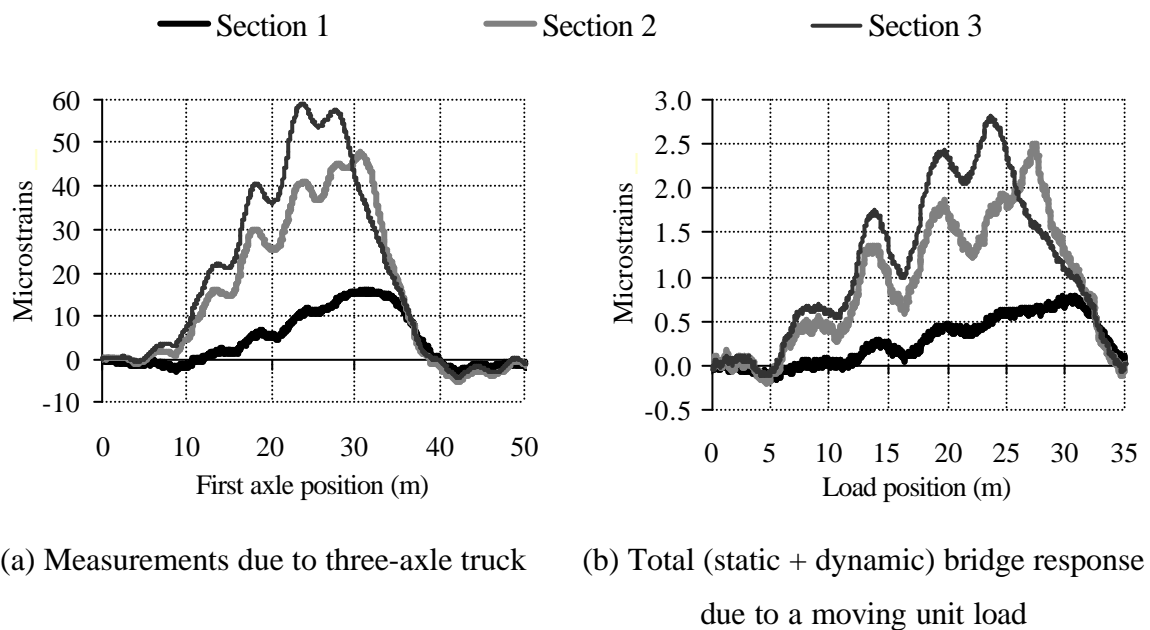


Figure 8.48 – Calibration of sections at 4, 8 and 12 m in southbound lane (Slovenia)

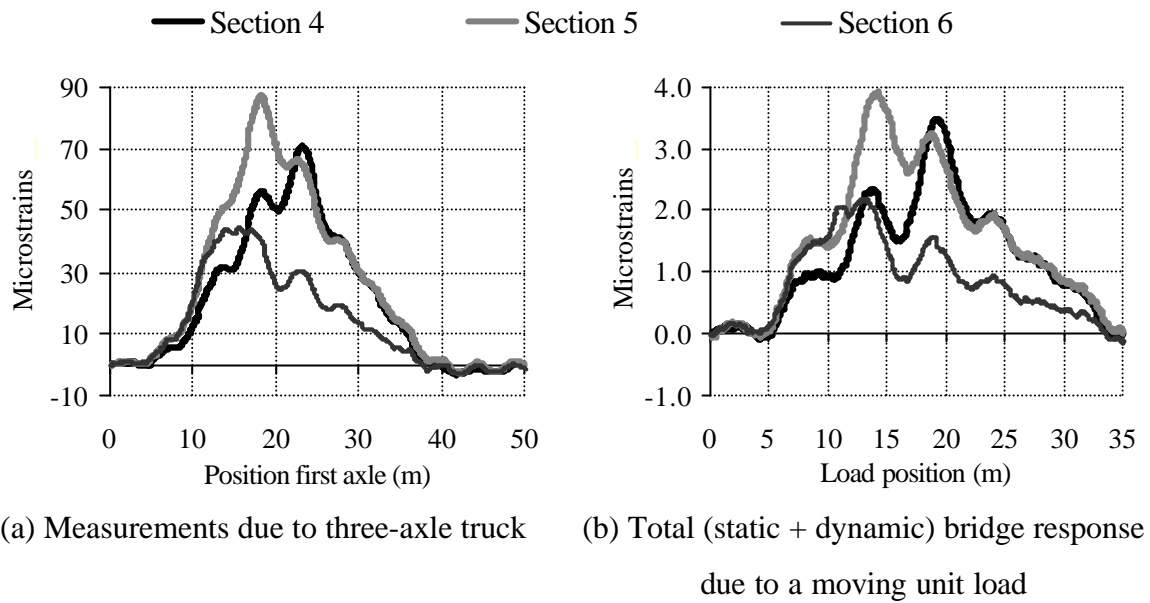


Figure 8.49 – Calibration of sections at 16, 20 and 24 m in southbound lane (Slovenia)

Finally, the load history is represented in Figure 8.50 (real static weights: 61.2 in the front axle and 178.7 kN in the rear tandem). Although calibration has taken place assuming equal load for second and third axles, the second axle appears to be heavier than the third axle from the bridge response and the solution given by the multiple-sensor system.

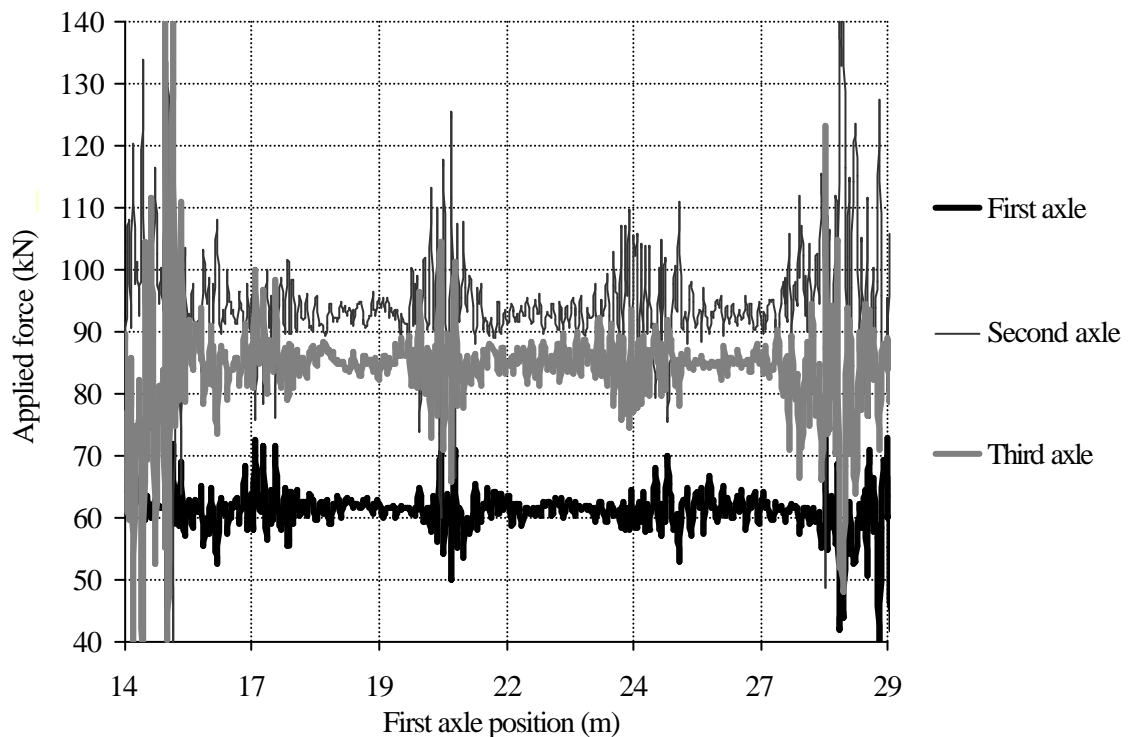


Figure 8.50 – Load history in southbound carriageway (Slovenia)

After first attempts by Kealy (1997), a load history has been reproduced from measurements in a B-WIM site successfully. The algorithm proves to be very accurate in the estimation of the static value from the average of the load history (Figures 8.47 and 8.50). Small errors of 2.6% and -0.57% have been obtained for the two-axle calibration truck in the front and rear axle weight respectively. The errors in the estimation of weights of the three-axle calibration truck have been 0.33% in the front axle and -0.09% in the rear tandem. A multiple-sensor B-WIM system can be a very accurate method of weighing trucks for some particular sites, but further investigation on the ideal number of sensors and their location, and experimental testing based on a wider range of vehicles and speeds are necessary.

8.6 CONCLUSIONS

Four bridges have been instrumented for B-WIM purposes and calibrated under different environmental conditions. An accuracy analysis of the calibration runs has been given according to the COST323 European specification (Appendix B). A new experimental procedure based on the frequency domain has been used to calibrate a B-WIM system by the first time. Apart from the traditional static algorithm, other two new algorithms, DB-WIM and MS-BWIM, have also been analysed with measurements from the field. Though the sample of trucks used to calibrate the system has been very small, first results on accuracy are promising. Further testing with a bigger population size is required in the near future.

The use of a 4 Hz hardware filter in Delgany and Luleå has been a significant source of inaccuracy. In spite of the filtering effect, the use of an experimental influence line based on a spectral calibration over a traditional calibration based on a theoretical beam model improved overall accuracy from E(55) to C(15) in Delgany (one calibration truck travelling with the same load at different speeds). Group of axles criterion also improved from D(25) to A(5). If only the runs at 70 km/h instead of all runs were considered, A(5) overall accuracy could be achieved. In Luleå, overall accuracy D+(20) was obtained using two trucks and different levels of speed. Overall accuracy A(5) could be obtained if using the same truck travelling several times at the same speed while overall accuracy B+(7) would result if using runs of two different trucks travelling at about the same speed. This

difference in accuracy depends on the speed and truck configuration and it is mainly a consequence of the filter. In Belleville, gross vehicle weight is predicted with DB-WIM in an accuracy class B(10), but results in group of axles or single axles are extremely poor. In Slovenia, MS-BWIM is used to depict the axle load history, which average value is very close to the real static weight.